GRANT
IN-46-CR
OCIT.

NASA-CR-194265

19413 1

THE UNIVERSITY OF MICHIGAN
DEPARTMENT OF ATMOSPHERIC, OCEANIC, AND SPACE SCIENCE
Space Physics Research Laboratory
2245 Hayward Street
Ann Arbor, Michigan 48109-2143

P 49

Contract/Grant Number	NAG8 858
Project Name	Remote Sounding of Tropospheric Minor Constituents

Report Author(s)	S. Roland Drayson	313/936-0484
Author(s) Phone	Paul B. Hays	313/764-7220
	Jinxue Wang	313/764-6579

Report Date	3 December 1993
Report Type	Final Technical Report
Period Covered	November 1990 through October 1992
Project Director:	S. Roland Drayson
Principal Investigator(s)	S. Roland Drayson Paul B. Hays Jinxue Wang
Program Technical Officer	Ronald J. Koczor
Address	Code ES41 George C. Marshall Space Flight Center Marshall Space Flight Center, AL 35812

TABLE OF CONTENTS

Abstract

The etalon interferometer, or Fabry-Perot interferometer (FPI), with its high throughput and high spectral resolution has been widely used in the remote-sensing measurements of the earth's atmospheric composition, winds, and temperatures. The most recent satellite instruments include the Fabry-Perot interferometer flown on the Dynamics Explorer-2 (DE-2) (Hays, 1981) and the High Resolution Doppler Imager (HRDI) (Hays, 1985) to be flown on the Upper Atmosphere Research Satellite (UARS). These instruments measure the Doppler line profiles of the emission and absorption of certain atmospheric species (such as atomic oxygen) in the visible spectral region. The successful space flight of DE-FPI and the test and delivery of UARS-HRDI have demonstrated the extremely high spectral resolution and ruggedness of the etalon system for the remote sensing of earth and planetary atmospheres. Recently, an innovative FPI focal plane detection technique called the Circle-to-Line Interferometer Optical (CLIO) system was invented at the Space Physics Research Laboratory (SPRL) (Hays, 1990). The CLIO simplifies the FPI focal plane detection process by converting the circular rings or fringes into a linear pattern similar to that produced by a conventional spectrometer, while retaining the throughput advantage of the etalon interferometer. CLIO makes the use of linear array detectors more practical and efficient with FPI, the combination of FPI and CLIO represents a very promising new technique for the remote sensing of the lower atmospheres of Earth, Mars, Venus, Neptune, and other planets. The Multiorder Etalon Spectrometer (MOES), as a combination of the rugged etalon and the CLIO, compares very favorably to other spaceborne optical instruments in terms of performance versus complexity.

In this report, the feasibility of an advanced etalon spectrometer for the remote sensing of tropospheric trace species, particularly carbon monoxide (CO), nitrous oxide (N_2O), and methane (CH_4) has been discussed. The etalon atmospheric spectroscopy techniques are described, instrument design and related technical issues are discussed. The primary objective is to establish the concept of atmospheric spectroscopy with the CLIO and etalon system and its applications for the measurements of tropospheric trace species, analyze system requirements and performance, determine the feasibility of components and subsystem implementation with available technology, and develop inversion algorithm for retrieval simulation and data analysis.

1.0 Introduction

1.1 Scientific Background

The troposphere is a region of great chemical diversity and activity, containing many important trace gases produced by natural and anthropogenic processes at the surface and within the troposphere. Those trace gases affect the chemistry of the entire atmosphere and directly impact the quality of the air we breathe, they also play important roles in the greenhouse effect. Carbon monoxide (CO), nitrous oxide (N_2O), methane (CH_4) are some of the important trace species. The measurements of those trace species are very important in our understanding and modeling of the atmosphere.

Carbon monoxide is one of the key trace species which are very important in the photochemistry and chemistry of the atmosphere. The concentration of CO in the earth's atmosphere has been increasing mainly because of the increased human activities (Khalil and Rasmussen, 1984). The full range of the effects of the increased concentration of CO is not fully understood at the present time, but it is believed that CO is photochemically active and directly impacts the concentration of OH radicals in the troposphere. It leads to the destruction of OH through the following reaction

$$OH + CO \rightarrow CO_2 + H\,. \tag{1.1}$$

Increased CO may deplete tropospheric OH radicals, thereby reducing the yearly removal of many natural and anthropogenic trace species. In particular, this effect may add to the increase of CH_4, which in turn could further reduce OH concentration by the following chemical reactions

$$OH + CH_4 \rightarrow CH_3 + H_2O\,. \tag{1.2}$$

Increased CO may also indirectly intensify global warming and perturb the stratospheric ozone layer by increasing the lifetimes of CH_4 and trace gases such as CH_3Cl, CH_3CCl_3 and CFCs. A detailed discussion of the sources, sinks, and photochemistry of the tropospheric CO can be found in the paper by Logan et al. (Logan *et al.*, 1981). The atmospheric lifetime of CO is short, on the order of weeks or months. The global cycle of atmospheric CO is at present poorly understood due to the lack of comprehensive global observations with adequate temporal and spatial resolutions. So there is a strong need to measure the global distribution of tropospheric CO.

Nitrous oxide and methane, with their strong bands in the thermal infrared, are important greenhouse gases (Dickinson and Cicerone, 1986). N_2O is produced by several microbial pathways and is both a greenhouse gas and a sink for tropospheric ozone. The dissociation products of N_2O in the stratosphere, NO_x, are involved in the destruction of ozone (Isaksen and Stordal, 1986). The amount methane in the atmosphere has more than doubled over the last 200 years, according to the ice-core data (Kalil and Rasmussen, 1987). Also, adding methane to the atmosphere is about 20 times more effective in raising global temperature than adding equal amounts of CO_2. Methane is a strong source of H_2O in the stratosphere. The reasons for the increase of CH_4 are mainly the following: increased emission from anthropogenically controlled sources (cattle and other ruminants, biomass burning, fossil fuel use, rice paddies, solid waste), and lagging destruction in the atmosphere due to the decrease of OH radicals induced by anthropogenic release of CO. The global concentration measurement of N_2O and CH_4 are some of the important objectives of the Global Tropospheric Chemistry Study program (Levine, 1987). The increase in the concentrations of N_2O and CH_4 has important implications for the atmosphere. Measurements of temporal and spatial variations of N_2O and CH_4 could yield important insights into their atmospheric cycles and how they interact with the surface, ocean and the land systems.

Like most tropospheric trace species, tropospheric CO, N_2O, and CH_4 concentrations are very difficult to measure globally by space-borne instruments. The first successful measurement of tropospheric CO was achieved by the Measurements of Air Pollution from Satellite (MAPS) program, a gas filter correlation radiometer in the nadir-viewing mode. The global mid-tropospheric concentration of CO was obtained during two flights of the space shuttle in 1981 (Reichle, 1986) and 1984 (Reichle, 1990). Recently, a more advanced instrument, the Tropospheric Radiometer for Atmospheric Chemistry and Environmental Research (TRACER), was proposed as an EOS instrument to obtain CO concentration at three levels in the troposphere (Reichle, 1989,1990). The TRACER also uses the gas filter correlation technique. The selected EOS instrument for global tropospheric CO measurement is the MOPITT (Measurements of Pollution in the Troposphere), it is basically a pressure modulator radiometer (Taylor, 1983). The objective of MOPITT is to measure the tropospheric CO profiles by monitoring its thermal radiation at 4.7 μm and total column of CH_4 and CO by measuring the solar radiation reflected from the surface. The upwelling CO thermal emission from different altitude regions of the atmosphere is selected by mechanically modulating the pressure of the gas in a cell containing CO. Although the instrument is relatively simple, but the understanding and modeling of the operation of the gas cell has been a problem. Despite the extensive use

of the technique, there has been little experimental work to verify the operation of the modulator, the complexities of the rapid expansion and compression of the gas and line formation within the cell present difficult problems (Drummond et al., 1990; May et al., 1988). Unless the operation of the gas cell is completely understood and the mechanical pressure modulation can be precisely controlled, the confidence of the CO measurement will be compromised, so independent measurements by other techniques seem to be necessary to provide the important data verification and inter-comparison. As for N_2O, there is no previous comprehensive global measurements.

The technique of atmospheric spectroscopy with the Fabry-Perot interferometer has many important and desirable features for space-borne high resolution atmospheric trace species remote sensing. The Fabry-Perot interferometer is a compact, rugged, and high resolution spectral dispersing device. It has a big throughput advantage, the Jacqinot advantage, compared with grating and other types of instruments. Historically, it has been widely used in astronomy, astrophysics, and Doppler shift measurements. Recently, it has been employed as space-borne instruments, such as DE-FPI, HRDI and CLAES (Roche, *et al.*, 1988) on the Upper Atmospheric Research Satellite (UARS). In both DE-FPI and HRDI, the Fabry-Perot etalons have been used in the visible region with special detectors, namely the Image Plane Detector (IPD) (Killeen, *et al.*, 1983), to measure the Doppler shift of the emission lines of certain atmospheric species (such as atomic oxygen). In CLAES, solid etalon with tilt scanning has been used. The capability of the Fabry-Perot etalon has not been fully utilized because of the use of tilt scanning strategy and the fact that the detectors are unable to collect all the energy within an interference fringe. Recently, a new device, the circle to line converter, has been invented (Hays, 1990). With this new device, a linear detector array at the focal plane will be able to collect all the energy within a number of Fabry-Perot fringes of interest. The combination of the Fabry-Perot etalon and the circle to line converter produces a very effective spectroscopic instrument for remote sensing applications. One of the possibility is the remote sensing of tropospheric trace species.

1.2 Objectives

It is well known that many atmospheric molecules have periodic spectrum, CO and N_2O are two of those molecules. The Fabry-Perot interferometer is an instrument with periodic passband. Therefore a new instrumentation technique exploiting the periodic characteristics of the Fabry-Perot interferometer transmission function and the uniform spectral line spacings of CO and N_2O is realized by matching the CO or N_2O spectrum with the Fabry-Perot interferometer over a selected spectral region. Since the instrument passbands are in exact correlation with the CO or N_2O spectral lines and reject the

contributions of other species to the signal, the interferences by other species are minimized. Because of the multiplexing of many periodic spectral lines, high spectral resolution is possible with good signal to noise. We would like to call such an instrument the Multi-Order Etalon Spectrometer (MOES). MOES could provide a better measurement of the tropospheric CO and N_2O concentrations, especially in the lower troposphere, by directly observing the CO thermal emission or absorption in the 4.67 μm band and N_2O thermal emission and absorption in the 7.84 μm band. This technique solves the ground emission dominance problem in the wide-band radiometers or spectrometers by selectively measuring the CO and N_2O thermal emission or absorption at almost identical parts of a series of uniformly spaced CO or N_2O spectral lines. CH_4 does not have a regular band structure, but it is always possible to use two order, that is matching two instrument passbands with two appropriately selected CH_4 spectral lines. Tropospheric temperature and moisture channels are also included in MOES to provide temperature profiles needed for the retrieval of CO, N_2O and CH_4.

The objective of this project is to further investigate the MOES technique and establish the concept of atmospheric spectroscopy with the CLIO and etalon system and its applications for the measurements of tropospheric trace species, select spectral bands and channels, analyze system requirements and performance, determine the feasibility of components and subsystem implementation with available technology, and develop inversion algorithm for retrieval simulation and data analysis.

2.0 MOES Technique and Instrument Concept

2.1 Fabry-Perot Interferometer

Fabry-Perot interferometer is a spectrally dispersing device consisting of two flat and transparent plates with multi-layered dielectric coatings of high reflectivity and low absorption on the internal surfaces, the two plates are held parallel to each other and form a resonant cavity. When the two plates have a fixed separation, the Fabry-Perot interferometer is often called a Fabry-Perot etalon. The collimated light entering the cavity is successively reflected between the plates by the dielectric coating (Fig. 2.1). The transmitted light beams are brought to a focus by a fringe forming lens placed at the exit. These beams interfere with each other constructively or destructively depending on the FPI operating wavelength. Spectral dispersion is accomplished by this multi-beam interferences. At certain wavelengths, constructive interference occurs, and all of the incident light is transmitted (in the absence of absorption), at other wavelengths, destructive interference occurs, and all the incident light is reflected (in the absence of absorption). The transmission function of a Fabry-Perot interferometer with perfectly flat surfaces exactly parallel to each other is given by the Airy function

$$T = \frac{(1-R)^2}{1-2R\cos(4\pi\mu\nu t\cos\theta)+R^2} \tag{2.1}$$

(Born and Wolf, 1975; Reynolds *et al.*, 1989), where R is the reflectivity of the dielectric coating, μ is the index of refraction of the material between the plates, ν is the wavenumber of the incident light, t is the gap thickness, and θ is the angle of incidence of the light in the cavity. Transmission maxima or constructive interferences occur when the following condition is met

$$4\pi\mu\nu t\cos(\theta) = 2\pi m, \text{ or } 2\mu\nu t\cos(\theta) = m, \tag{2.2}$$

where m is called the order of interference. For a monochromatic incident light beam at wavenumber ν with a fixed gap thickness at t and index of refraction at μ, the transmitted light forms a series of concentric rings on the focal plane (Fig. 2.2). Each ring corresponds to a transmission maxima or a different value of m, this is the spatial periodicity of FPI. There is also a spectral periodicity characteristics. The typical FPI transmission function is illustrated in Fig. 2.3, each peak here corresponds to a different wavenumber (or wavelength). The transmission function is perfectly periodic with respect

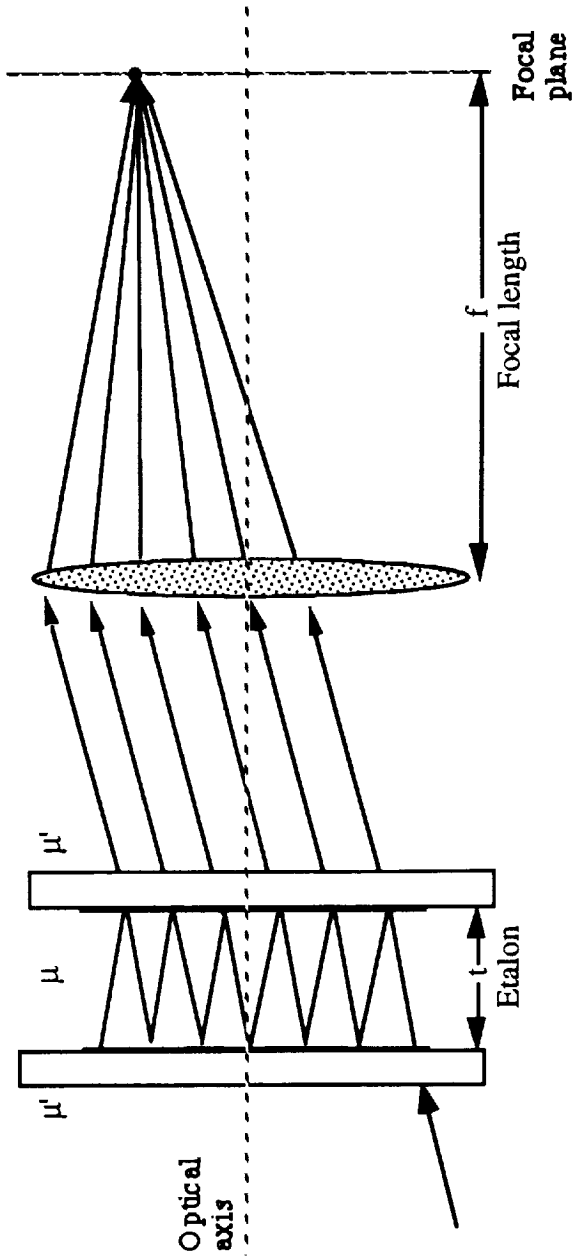

Fig. 2.1. Schematic diagram of multiple-beam interference in a Fabry-Perot interferometer. The collimated light entering the cavity is successively reflected between the plates by the diaelectric coating, and the transmitted light beams are brought to focus by a fringe forming lens at the exit to produce the concentric fringe pattern.

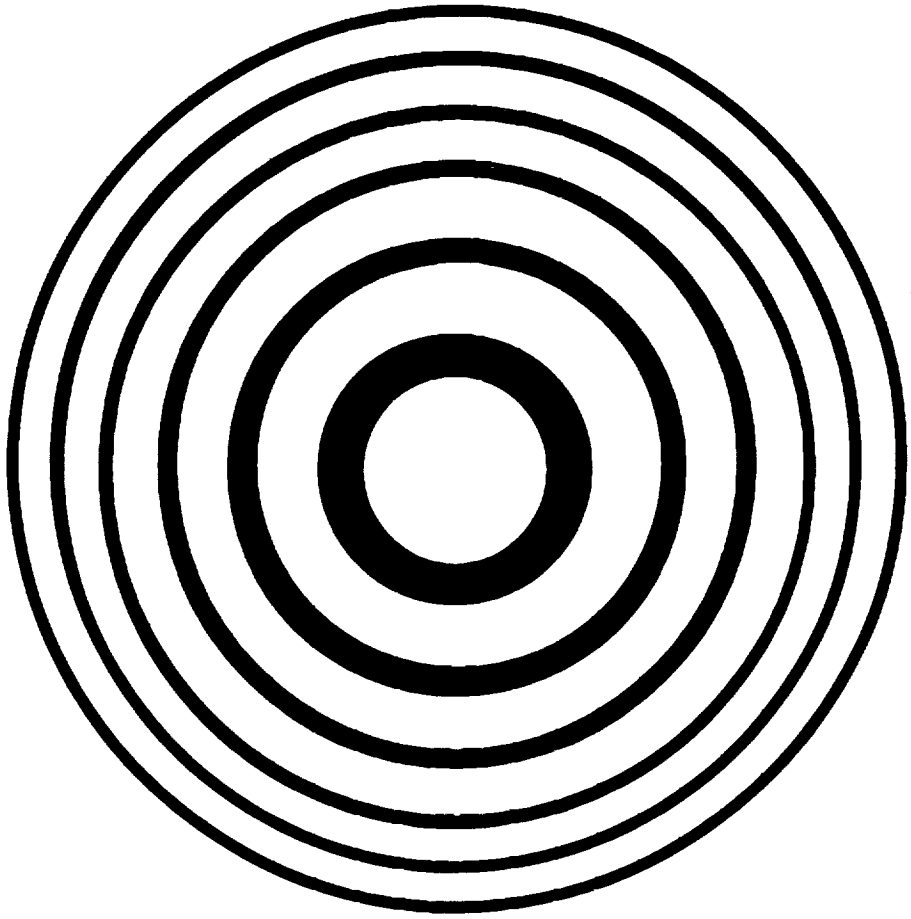

Fig. 2.2. Fabry-Perot interferometer ring pattern at the focal plane. The rings are corresponding to the transmission maxima or constructive interferences of the multiple-beam from the etalon. All the rings are equal area.

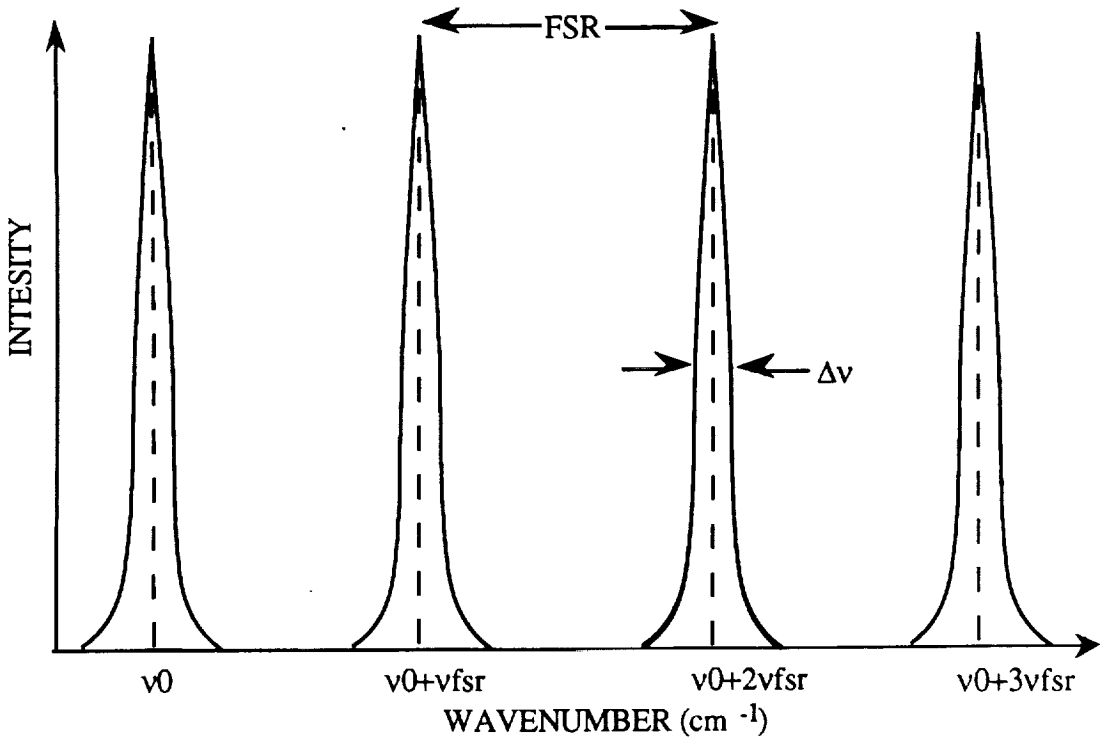

Fig. 2.3. Fabry-Perot interferometer transmission function. It is of high spectral resolution and periodic with a period of the free spectral range ν_{fsr}. The bandwidth $\Delta\nu = \nu_{fsr}/N_F$, N_F is the effective finesse of the interferometer.

to wavenumber, each transmission peak is called one order. This is one of the unique characteristics of the FPI that we are going to exploit in the design of MOES. The distance between two neighbor peaks or orders in the spectral domain is known as the free spectral range

$$\nu_{fsr} = \frac{1}{2\mu t}, \tag{2.3}$$

where ν_{fsr} is the free spectral range in wavenumber. Physically, ν_{fsr} can be described as the change in wavenumber required to move from one transmission peak to the next transmission peak. The sharpness of those rings or equivalently the sharpness of the transmission peaks, which can be described by the full width at half maximum (FWHM) of the Airy function peaks, is closely related to the reflectivity of the etalon. The relationship between $\Delta\nu$, R, and ν_{fsr} is given by the following formula

$$\Delta\nu = \frac{(1-R)}{\pi\sqrt{R}}\nu_{fsr} \tag{2.4}$$

(Jacquinot, 1960). The reciprocal of the first part of the expression is defined as the reflectivity finesse N_R (Jacobi, 1958; Hernandez, 1986)

$$N_R = \frac{\pi\sqrt{R}}{1-R}, \tag{2.5}$$

which is what would be found for ideally flat etalon plates with no defects at reflectivity R. In practice the instrumental function and finesse will be modified by plate imperfections, and we can define an effective instrument finesse as N_E. The FWHM of the transmission peaks or the spectral resolution of the etalon can be expressed as

$$\Delta\nu = \frac{\nu_{fsr}}{N_E}. \tag{2.6}$$

With a fixed ν_{fsr}, the higher the instrument finesse N_E, the higher the spectral resolution of the etalon.

2.2 The Circle to Line Interferometer Optical (CLIO) System

As mentioned before, the Fabry-Perot etalon creates a series of rings at the infinite focus of the system, and special detectors and scanning strategies are needed to analyze the circular interference fringes and extract useful spectral information. The Circle to Line Interferometer Optical System (CLIO) (Hays, 1990), which we plan to use in MOES, will convert the circular rings or fringes into a linear pattern similar to that produced by a conventional spectrometer, while retaining the basic throughput advantage of the Fabry-Perot interferometer. The resulting linear fringe pattern can be measured by using the commercially available linear array detectors, a great advantage over the use of the costly and rather inflexible special purpose detectors, such as the Image Plane Detector used in Dynamics Explorer (DE) Fabry-Perot interferometer. Furthermore, detectors of the IPD type are not feasible for the infrared region at the present time. The basic optical configuration of the CLIO is illustrated schematically in Fig. 2.4. By placing a 45 degree cone at the focal plane, the series of rings are converted into a series of spots on the optical axis. But the cone project only one quarter of the ring effectively onto a detector element,

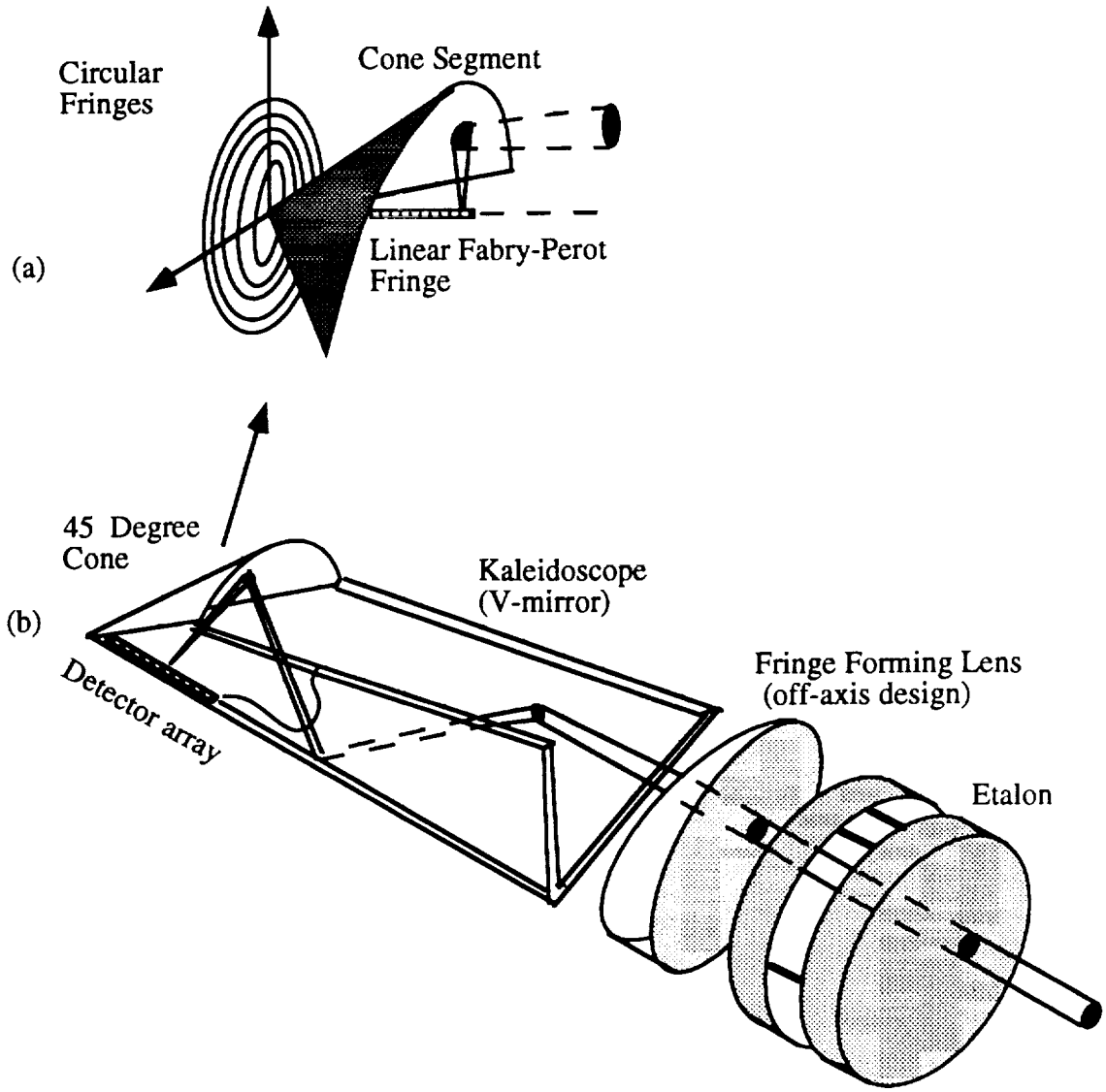

Fig. 2.4. (a) Illustration of the conversion of a ring segment into a spot by the cone; (b) the schematic diagram of the circle to line interferometer optical system.

while three fourths of the signal is lost. This problem is solved by using a mirrored Kaleidoscope which consists of a pie shaped segment of a telescopic objective enclosed by two mirrors joined at the optical axis of the lens system and terminated by the cone. The function of the Kaleidoscope is to transform an entire circular ring into a ring segment which is subsequently focused onto a detector element by the cone. A laboratory demonstration of the CLIO at SPRL of the University of Michigan generated good results and agrees well with theoretical predictions (Hays, 1990). The CLIO is an elegant, rugged device which could open the door for the use of infrared linear array detectors in IR-FPI.

The combination of CLIO and high quantum efficiency solid state detectors makes the Fabry-Perot interferometer more practical and efficient in atmospheric remote sensing. Because the circular fringes are converted by the cone and kaleidoscope into linear fringes on the conjugate focal plane, commercially available linear array detectors can be used. As will be shown later, the CLIO is an essential part of the multiorder etalon sounder (MOES).

2.3 Etalon Spectrometer Concept

The MOES technique exploits the periodic characteristics of the FPI transmission function, and the uniform spectral line spacings of many atmospheric molecules with a periodic spectrum (e.g., CO_2, CO, N_2O, *etc.*) to achieve high spectral resolution and maximize instrument signal to noise. Figure 2.5 again shows the multi-beam interference in a FPI, the concentric ring pattern on the focal plane, and the FPI periodic transmission function. Clearly it is periodic and of very high spectral resolution. As pointed before, the full width at half-maximum (FWHM) of each passband is determined by the free spectral range ν_{fsr} and the finesse N_E and is given by $\Delta\nu = \nu_{fsr}/N_E$. If the periodic FPI passbands fall in exactly the same relative position on a series of uniformly spaced spectral lines, the signal received through the interferometer has the same information as that received with a single very high resolution measurement of a single spectral line, but the signal level is increased by a factor equal to the number of orders being used. By matching the period of the FPI with the spacing of those spectral lines, high spectral resolution as well as high signal level can be achieved. Since the instrument passbands are in exact correlation with the spectral lines being sampled and reject the contributions of other species to the signal, the interference by other species is minimized. The MOES concept is further explained in Fig. 2.6. The upper panel shows the periodic spectrum of a band of interest (such as the P or R branches of CO band at 4.67 μm) being observed with a single passband instrument (such as a conventional spectrometer or radiometer). Note that the output signal is too weak for any meaningful interpretation. The lower panel shows the method of observation with a periodic passband instrument (such as the Fabry-Perot interferometer). In this case the signal is much stronger and the spectral line can be better resolved. Multiplexing of a number of CO spectral lines by a periodic passband instrument, such as MOES, results in higher signal-to-noise, which makes the use of higher spectral resolution possible. Narrower instrument channel weighting functions and better vertical resolution can be achieved because of higher spectral resolution.

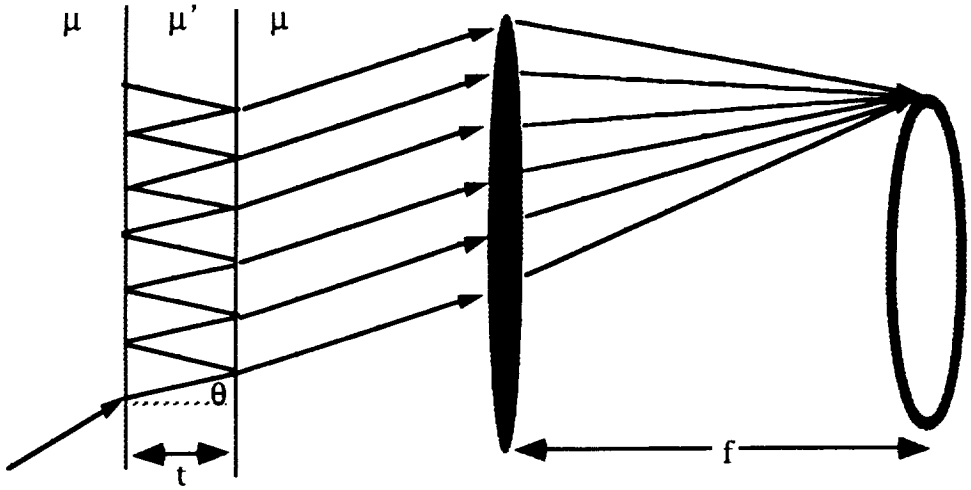

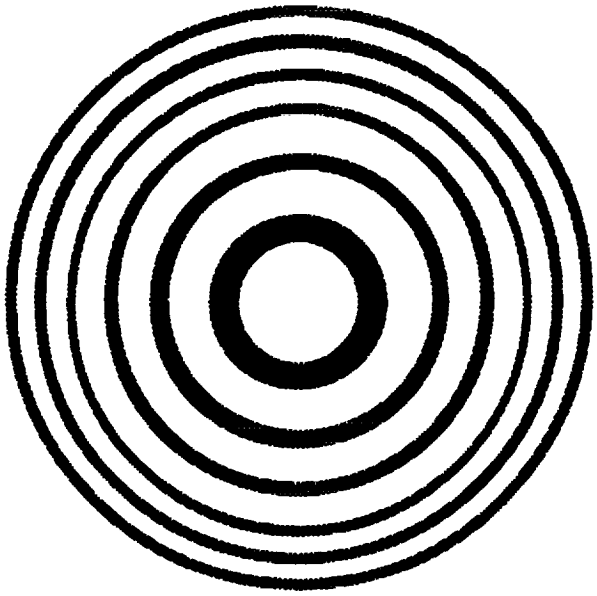

FPI Ring Pattern at Focal Plane

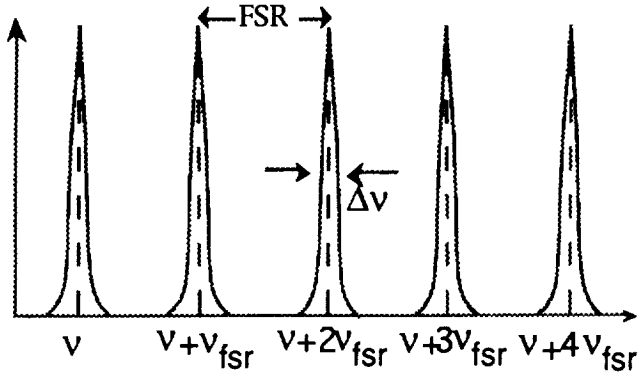

FPI Transmission Function

Fig. 2.5. Multiple-beam interference in a Fabry-Perot interferometer, the concentric ring pattern on the focal plane, and the FPI transmission function.

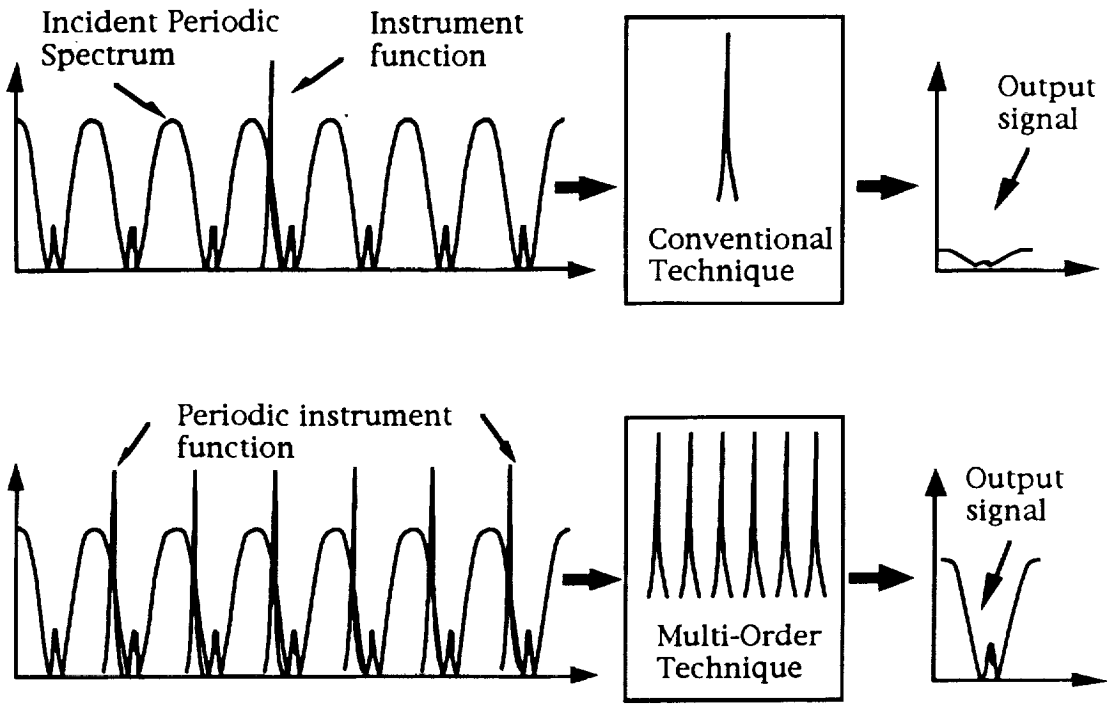

Fig. 2.6. Illustration of the observations of a periodic spectrum by a single-order conventional instrument and a multiorder periodic instrument (such as the Fabry-Perot interferometer).

3.0 Science and Measurement Requirements

MOES has the potential to measure many tropospheric and stratospheric trace species, but our efforts here will be focused on the measurements of tropospheric CO, N_2O, and CH_4, and the selection of appropriate spectral bands and channels will be for that purpose. Spectral channels are also included to measure the thermal emission or absorption by CO_2 and H_2O to provide the temperature profile which is needed for the retrieval of CO, N_2O and CH_4. The tropospheric temperature and moisture channels are optional depending on the availability of temperature and moisture profiles from other sources.

3.1 Channel Selections and Requirements for Tropospheric Carbon Monoxide (CO) Measurement

In choosing the appropriate spectral band, we need to consider the strength and uniformity of the CO spectral lines, and minimum interferences by other species. The major interference species in the 4.67 μm band of CO are O_3 and N_2O. The P-branch of the CO band is almost exactly overlapped by the 4.8 μm ozone band which consists of a

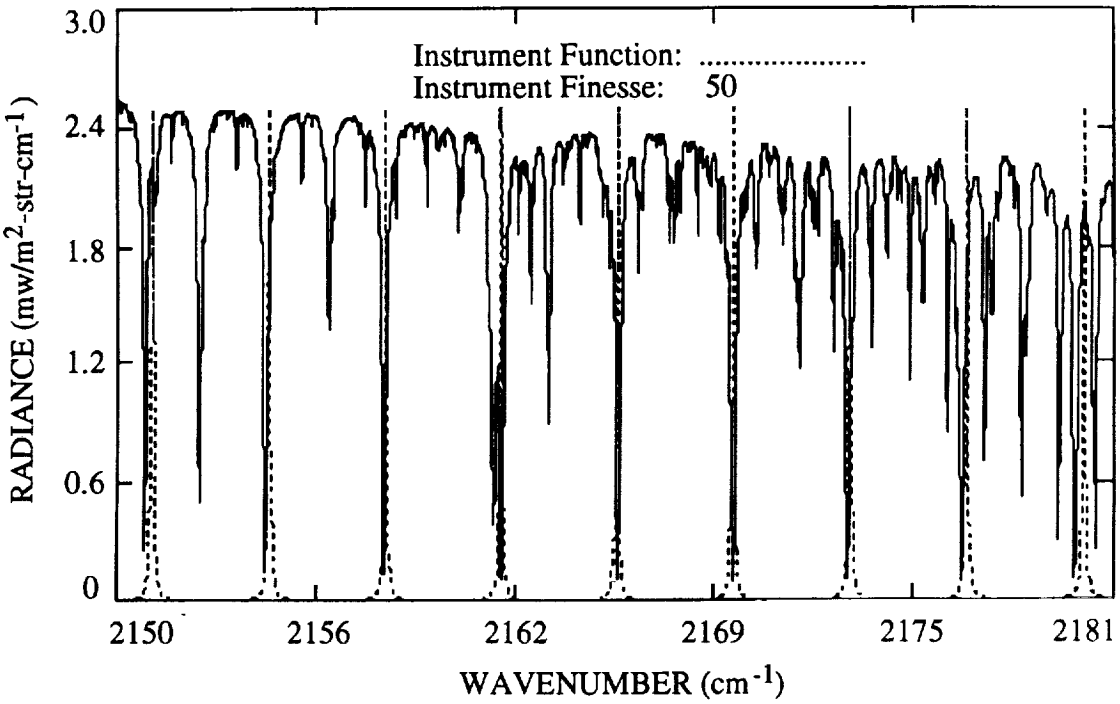

Fig. 3.1. Upwelling atmospheric radiance in the MOES CO sounding band with 9 orders and FPI instrument function with a finesse of 50.

large number of weak lines. Therefore even though the signal is stronger in the P-branch, it is advantageous to choose the R-branch of the CO band. Another important consideration is the number of orders to be used. Instrument signal level is proportional to the number of instrument orders, but the effective instrument spectral resolution will be reduced with many orders. This is due to the fact that the CO spectrum is not perfectly periodic, the line spacing changes across the band mainly due to the nonrigidity of the oscillator (Herzberg, 1950). This nonuniformity is also inversly proportional to the momentum of initia of the molecule. For example, CO_2 is heavier and has a bigger moment of initia than CO, its line uniformity is better than CO. In the case of CO_2, instrument order of 10-15 can be used without greatly reducing the effective instrument spectral resolution. In the case of CO, the use of nine order will reduce the effective instrument spectral resolution to about 0.5 cm^{-1} which is too low for tropospheric CO profiling. Fig. 3.1 shows the upwelling CO thermal radiation in a spectral region containing 9 strong regular CO lines, the MOES instrument function with an etalon finesse of 50 and the appropriate free spectral range to match the 9 CO spectral lines is also included as the dotted curve. Good match between the instrument function and CO spectral lines is achieved close to the band center (between 2162.0 cm^{-1} and 2169.0 cm^{-1}), but the

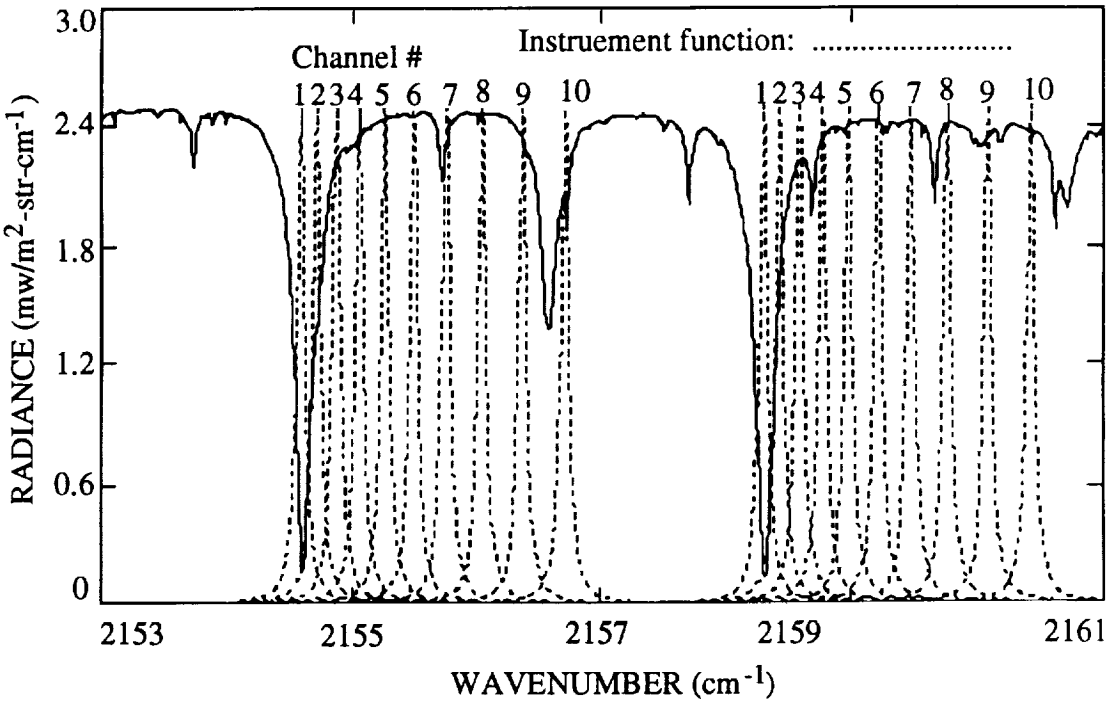

Fig. 3.2 Upwelling atmospheric radiance in the MOES CO sounding band with 2 orders and 10 channel instrument functions with a finesse of 50.

matchbecomes worse as one moves away from the band center. Orders close to the edge of the band, instead of falling on the center of the corresponding CO lines, the instrument passbands fall almost on the wing of the CO lines. This situation results in an effective instrument spectral resolution in the order of 0.5 cm^{-1}. Therefore if very high spectral resolution is desired, fewer orders have to be used. The lost of signal due to fewer orders can be compensated by longer integration time which is available on the GOES platform. In our study here, we choose two orders to achieve the highest spectral resolution and smallest interferences by other species possible with MOES. Two CO lines centered at 2154.596 cm^{-1} (4.641 μm) and 2158.300 cm^{-1} (4.633 μm) will be measured by MOES with an effective spectral resolution of 0.074 cm^{-1} (free spectral range ν_{fsr} = 3.708 cm^{-1}, etalon finesse N_f = 50). The upwelling atmospheric radiance around the two CO lines and the MOES instrument functions of ten CO sensing channels are shown in Fig. 3.2.

The weighting functions and contribution functions of the 10 MOES CO sounding channels and the upwelling atmospheric radiance in the CO sounding band (from 2152.0 cm^{-1} to 2161.0 cm^{-1}) with different CO profiles have been calculated and will be presented next. The purpose of those calculations is to show how sensitive the upwelling atmospheric radiance in the chosen band and the instrument weighting and contribution functions to the change of atmospheric CO profiles. Figure 3.3(a) shows the upwelling

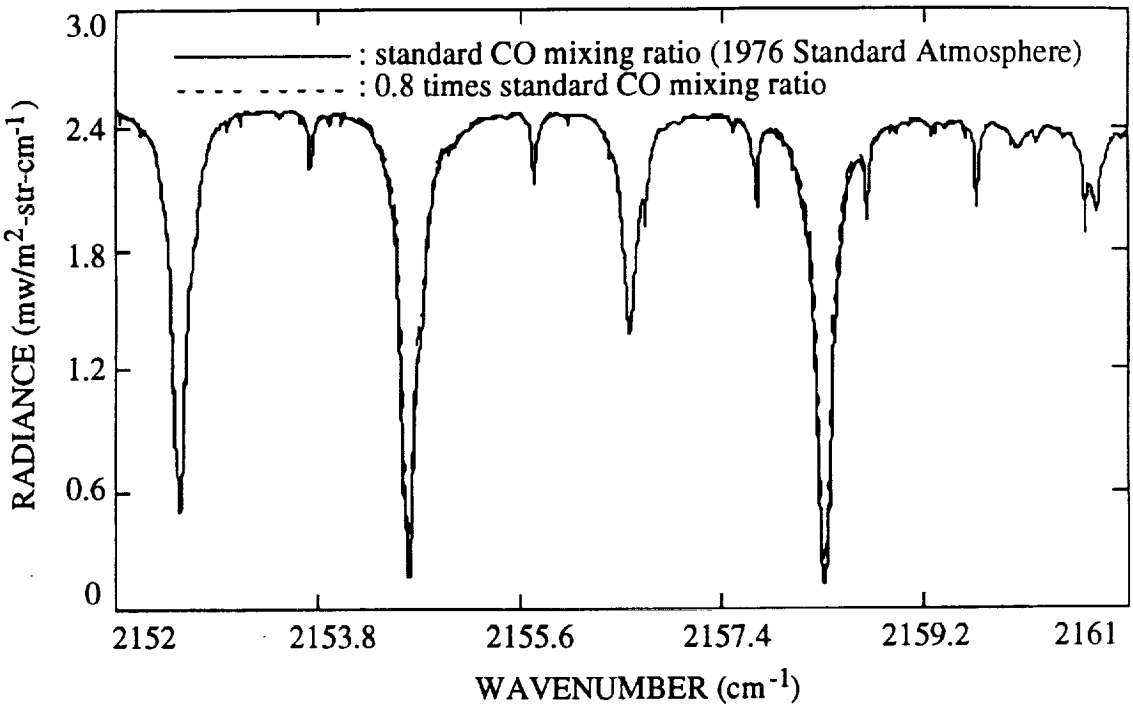

Fig. 3.3(a) Upwelling atmospheric radiance in the MOES CO sounding band with standard CO mixing ratio (1976 U. S. Standard Atmosphere) and 0.8 times standard CO mixing ratio. The mixing ratios of other interfering species (CO_2, H_2O, O_3, N_2O, CH_4, O_2) are the 1976 U. S. Standard Atmosphere profiles.

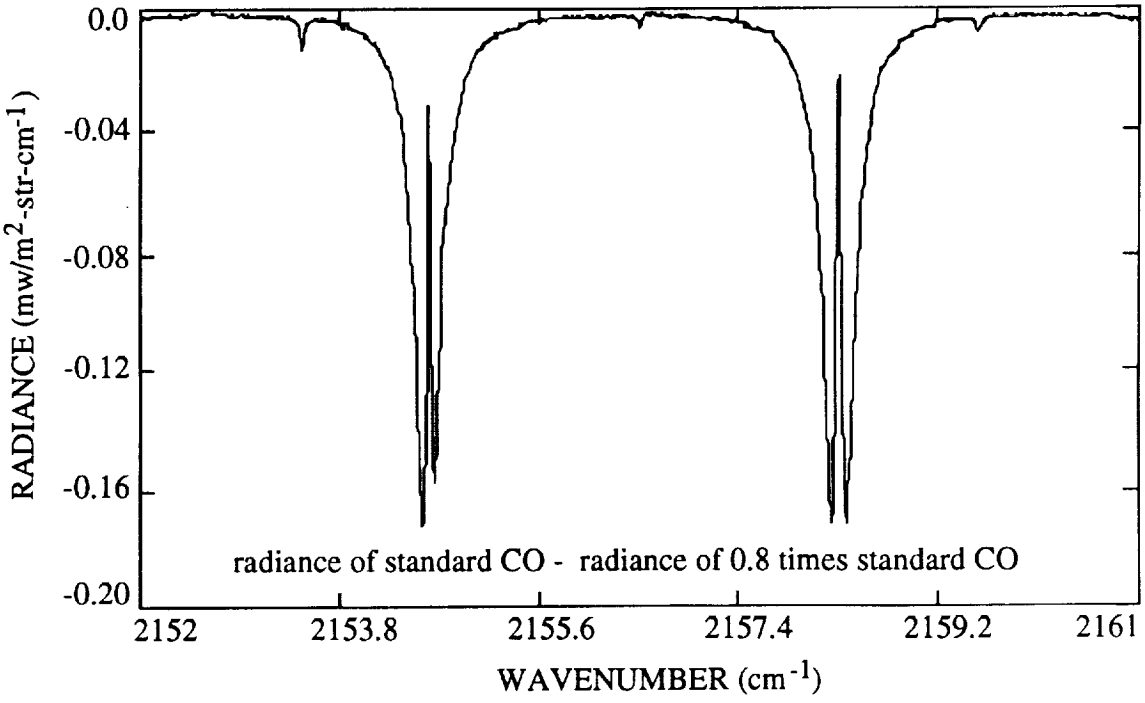

Fig. 3.3(b) Difference in the upwelling atmospheric radiance in the MOES CO sounding band with standard CO mixing ratio (1976 U. S. Standard Atmosphere) and 0.8 times standard CO mixing ratio.

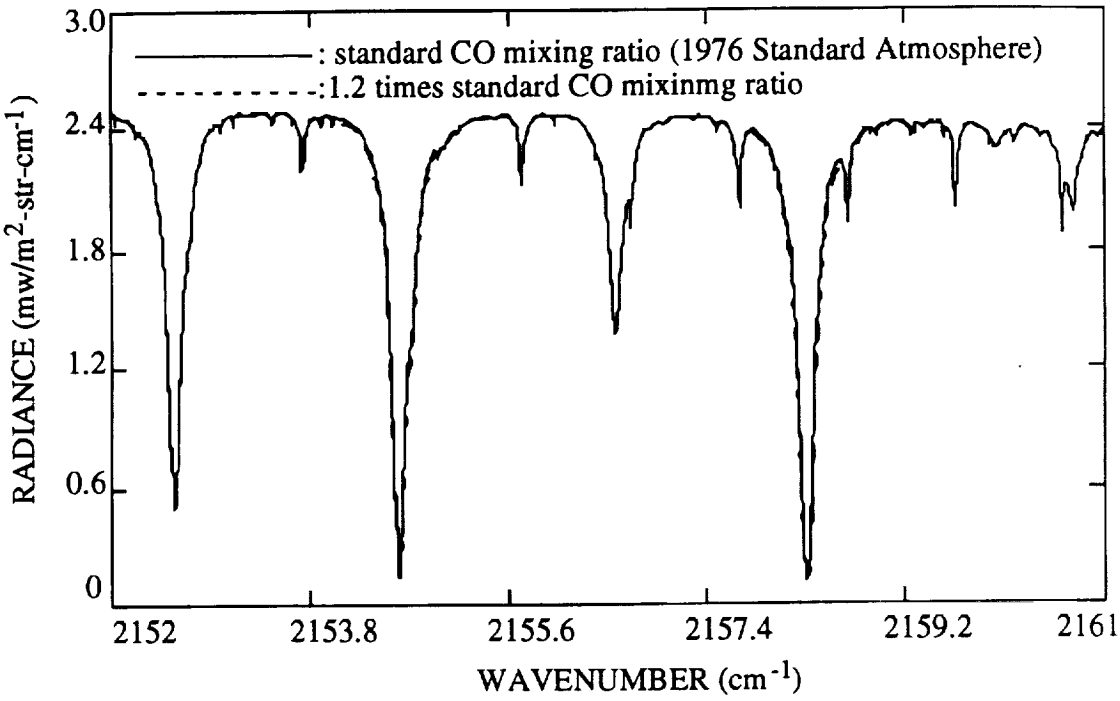

Fig. 3.4(a) Upwelling atmospheric radiance in the MOES CO sounding band with standard CO mixing ratio (1976 U. S. Standard Atmosphere) and 1.2 times standard CO mixing ratio. The mixing ratios of other interfering species (CO_2, H_2O, O_3, N_2O, CH_4, O_2) are the 1976 U. S. Standard Atmosphere profiles.

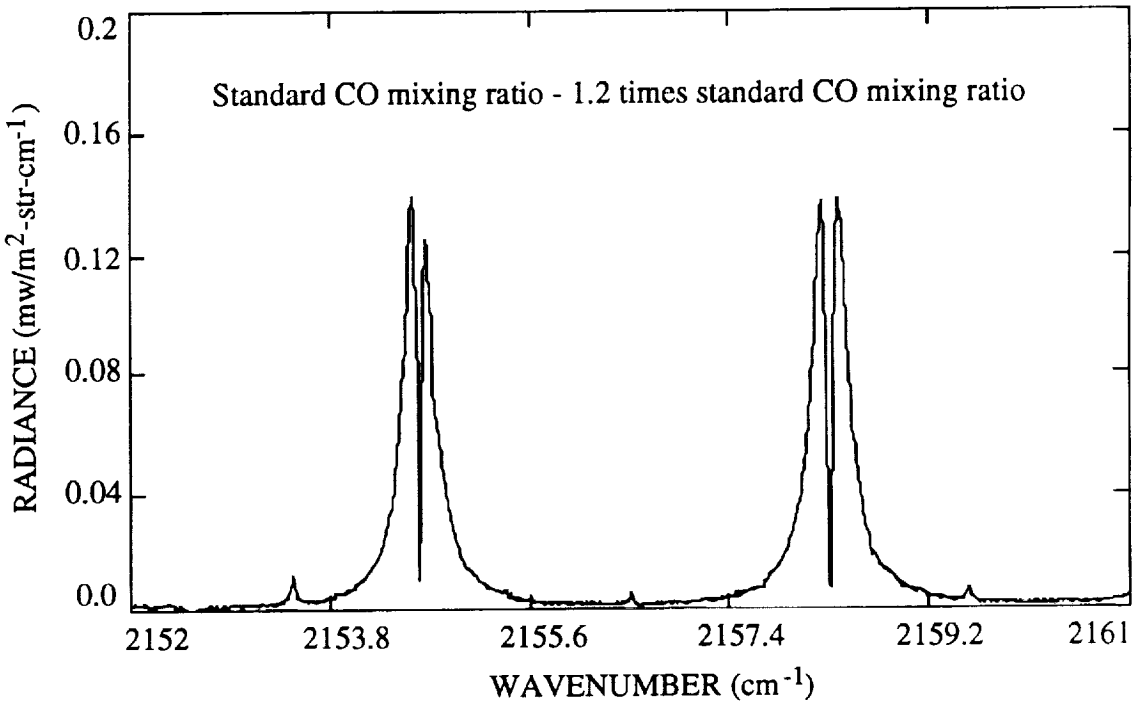

Fig. 3.4(b) Difference in the upwelling atmospheric radiance in the MOES CO sounding band with standard CO mixing ratio (1976 U. S. Standard Atmosphere) and 1.2 times standard CO mixing ratio.

atmospheric radiance in the chosen CO sensing band calculated with the 1976 U.S. Standard atmospheric CO profile, and 0.8 times the standard profile. Figure 3.3(b) shows the difference in the upwelling between 0.8 times the standard profile and the standard profile. Figure 3.4(a) shows the upwelling atmospheric radiance in the chosen CO sensing band calculated with the 1976 U.S. Standard atmospheric CO profile, and 1.2 times the standard profile. Figure 3.4(b) shows the difference in the upwelling between 1.2 times the standard profile and the standard profile. The mixing ratio of other interference species (H_2O, O_3, CO_2, CH_4, and N_2O) in all the calculations are the 1976 U.S. Standard profiles. Clearly, the radiance in the line wings are dominated by surface emission and are not sensitive to the changes of the CO profile, the radiance in the line center are most sensitive to the changes of CO profiles. Figure 3.5-3.7 show the weighting and contribution functions of the ten CO sounding channels with different CO mixing ratio profiles. The shapes and peaking altitudes are sensitive to the change of the CO profile. This indicate that useful information about the distributions of CO could be derived from those measurements. The retrieval of CO profile from MOES measurements will be further discussed later.

3.2 Channel Selections and Requirements for Tropospheric Nitrous Oxide (N_2O) Measurement

Similar to the selection of CO sounding band and channels, the selection of N_2O sensing band and channels also involves the consideration of interferences by other species and solar radiation, signal level, effective spectral resolution, and the availability of the very narrow band blocking filter. In the evaluation of interferences by solar radiation and other species, we have calculated the upwelling atmospheric radiance in several N_2O bands. The first band is from 2222.0 cm^{-1} to 2272.0 cm^{-1} which is the major N_2O sensing band of the proposed AIRS on EOS. In all the following atmospheric radiance and transmittance calculations, the 1976 U.S. Standard Atmosphere and line-by-line integration method have been used. Figure 3.8 shows the upwelling atmospheric radiance with a N_2O-only atmosphere (no interference by any other species), Fig. 3.9 shows the upwelling atmospheric radiance with 7 atmospheric molecules (N_2O, H_2O, O_3, CO, CH_4, CO_2, O_2) in the line-by-line calculations. Clearly, in this spectral band CO_2 is dominant beyond about 2230.0 cm^{-1}, it will be rather difficult to get any N_2O distribution information in the CO_2 dominated spectral region. Therefore the 7 channels between 2232.0 cm^{-1} and 2272.0 cm^{-1} will not be very effective for N_2O sensing. Due to the serious interference by other molecules, especially CO_2, in the spectral region 2222.0 cm^{-1} to 2272.0 cm^{-1}, we will not

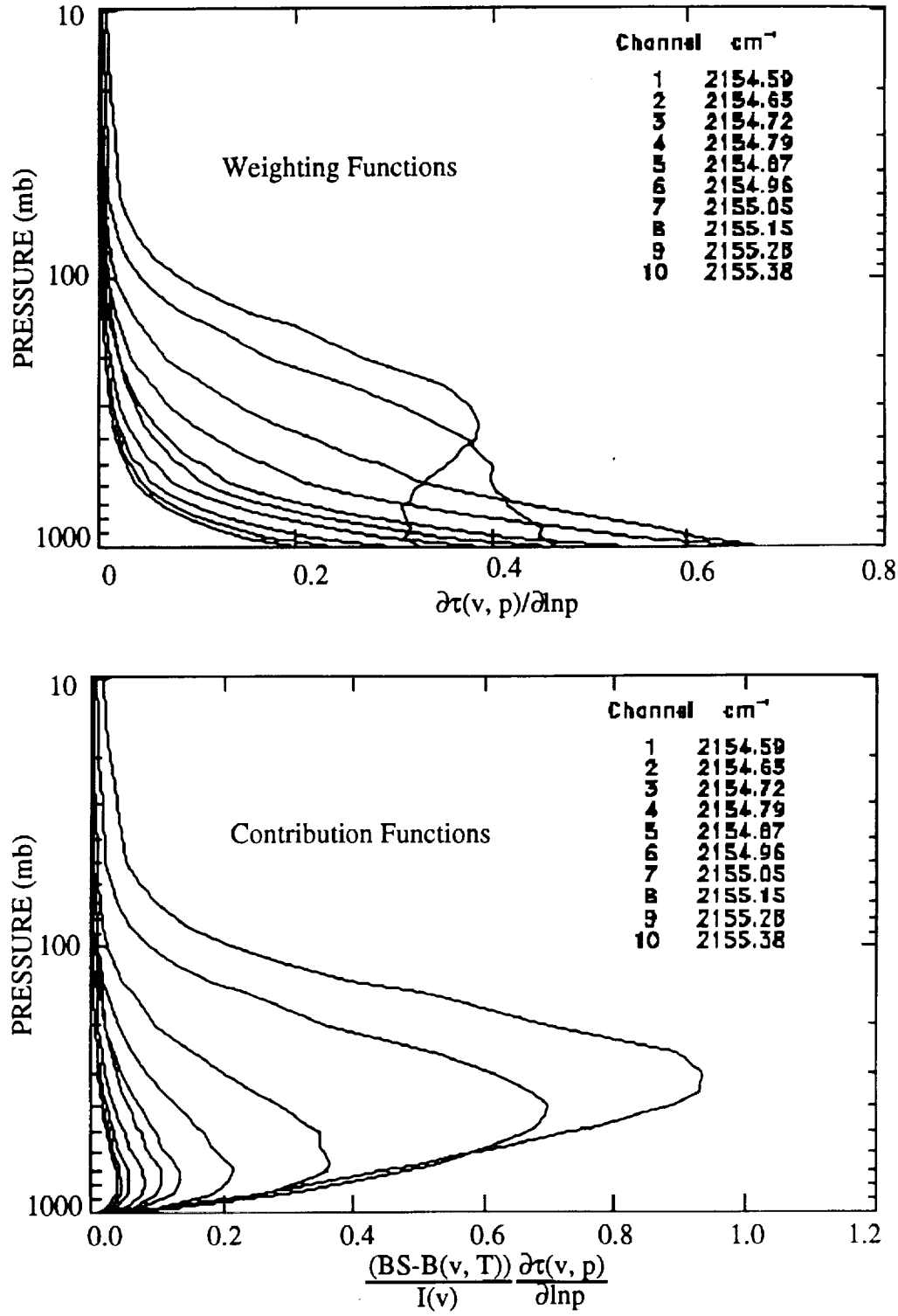

Fig. 3.5 Weighting and contribution functions of the 10 MOES CO sensing channels with 0.8 times the 1976 standard CO mixing ratio and instrument finesse of 50. BS is the surface contribution to the upwelling radiance, I(v) is the radiance "measured" by MOES.

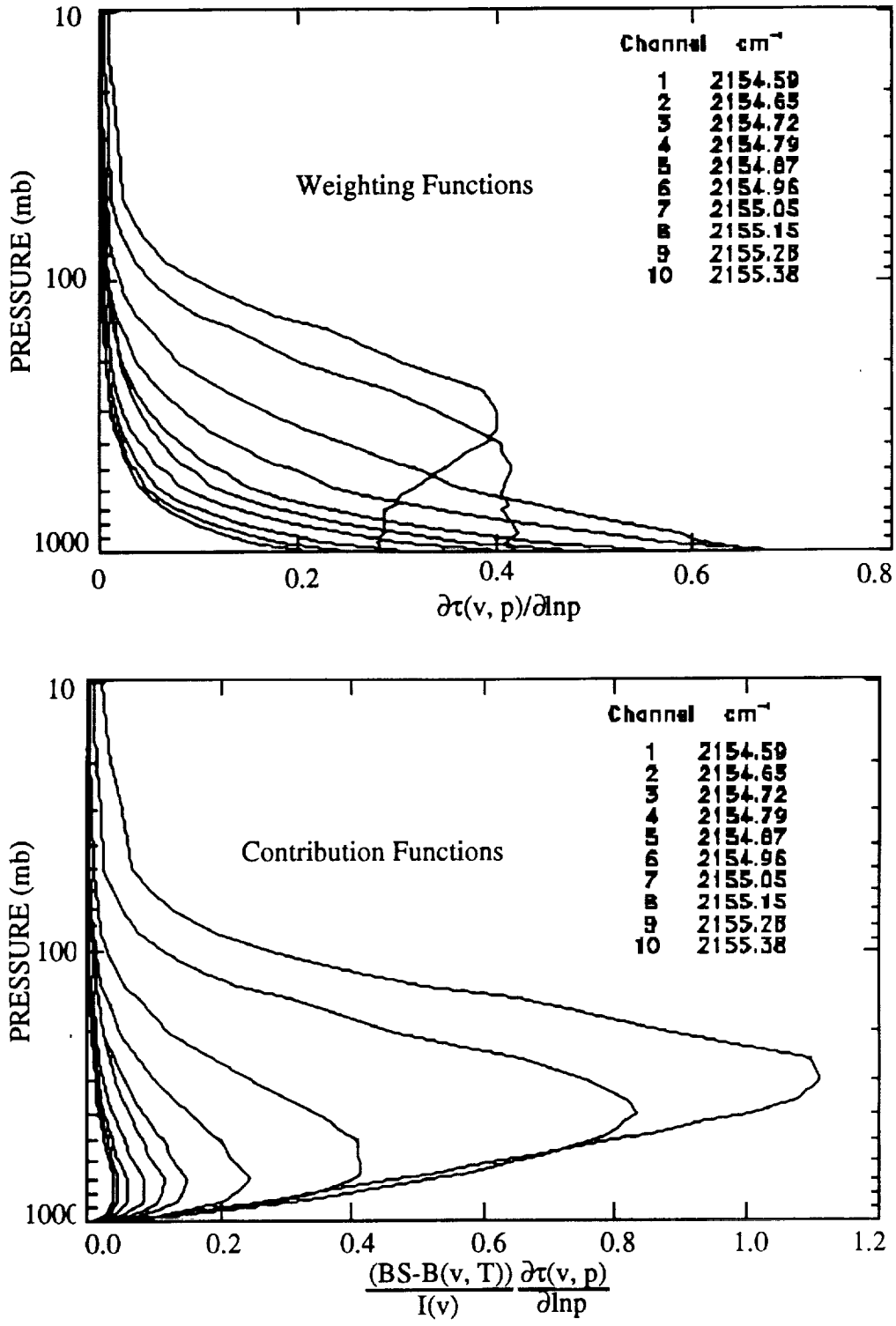

Fig. 3.6 Weighting and contribution functions of the 10 MOES CO sensing channels with the 1976 standard CO mixing ratio and instrument finesse of 50. BS is the surface contribution to the upwelling radiance, I(v) is the radiance "measured" by MOES.

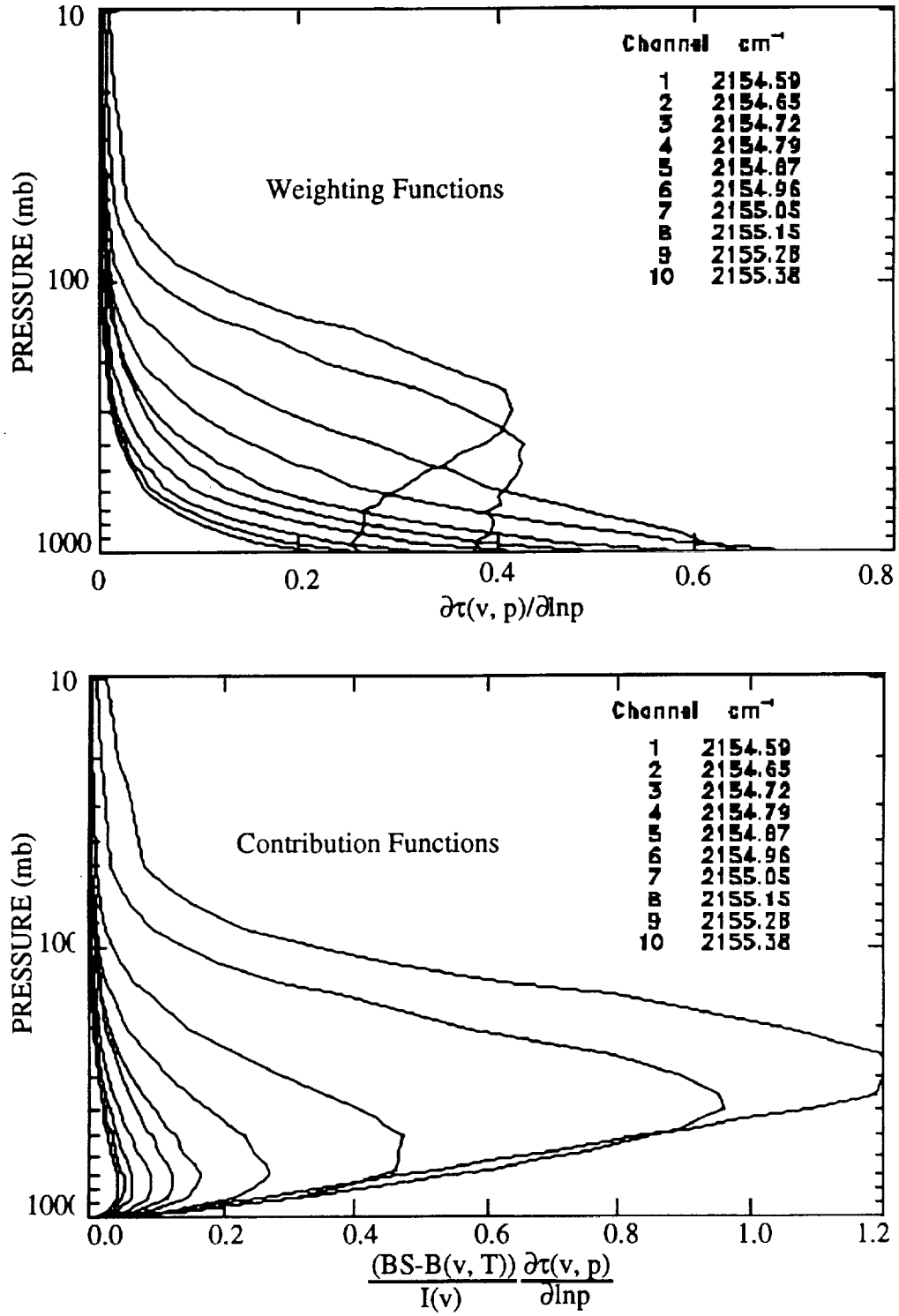

Fig. 3.7 Weighting and contribution functions of the 10 MOES CO sensing channels with 1.2 times the 1976 standard CO mixing ratio and instrument finesse of 50. BS is the surface contribution to the upwelling radiance, I(ν) is the radiance "measured" by MOES.

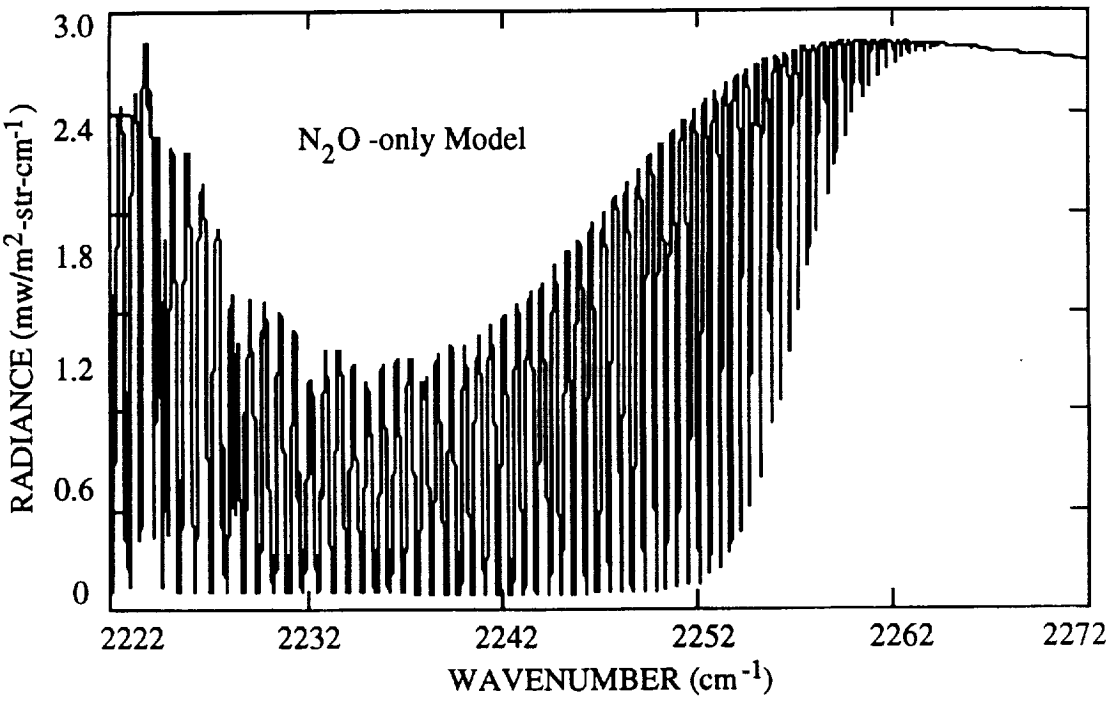

Fig. 3.8 Upwelling atmospheric radiance in N_2O band without interferences by other species. 1976 U. S. Standard Atmosphere and N_2O profile have been used in the calculation.

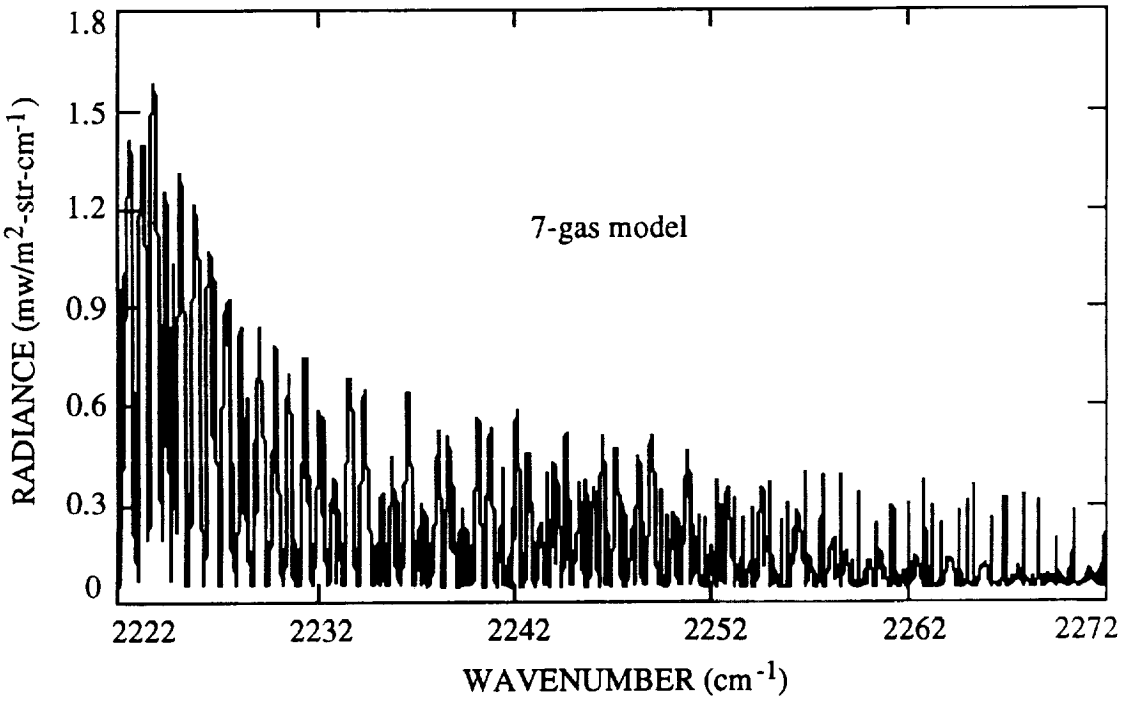

Fig. 3.9 Upwelling atmospheric radiance in N_2O band with interferences by other species. 1976 U. S. Standard Atmosphere and N_2O profile have been used in the calculation.

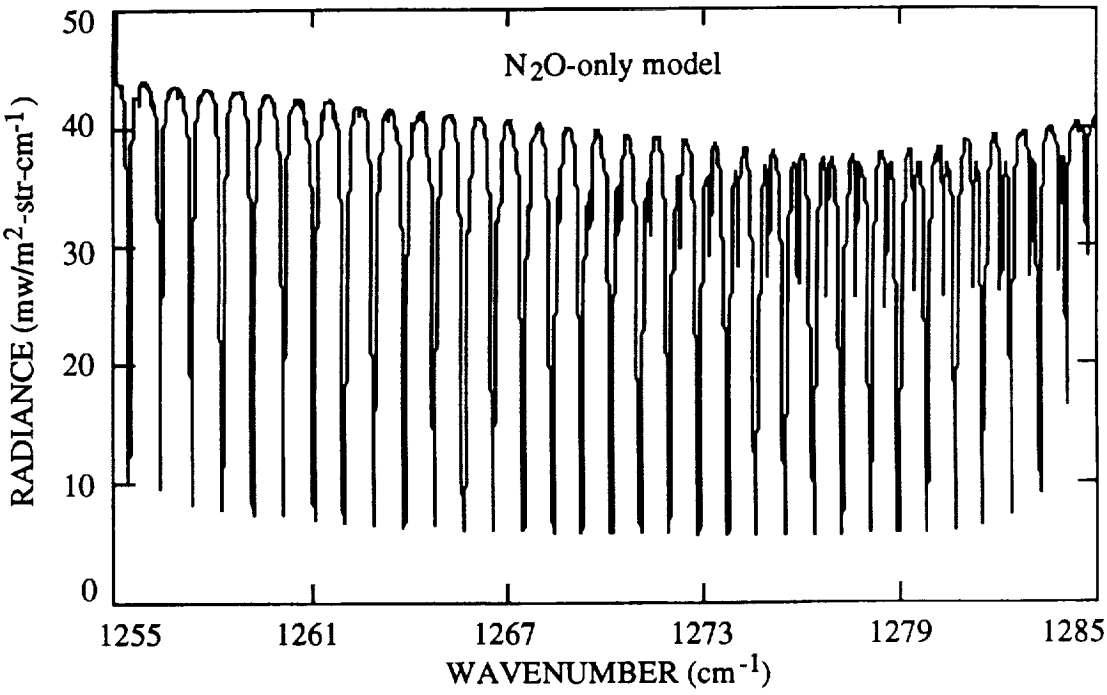

Fig. 3.10 Upwelling atmospheric radiance in N_2O band without interferences by other species. 1976 U. S. Standard Atmosphere and N_2O profile have been used in the calculation.

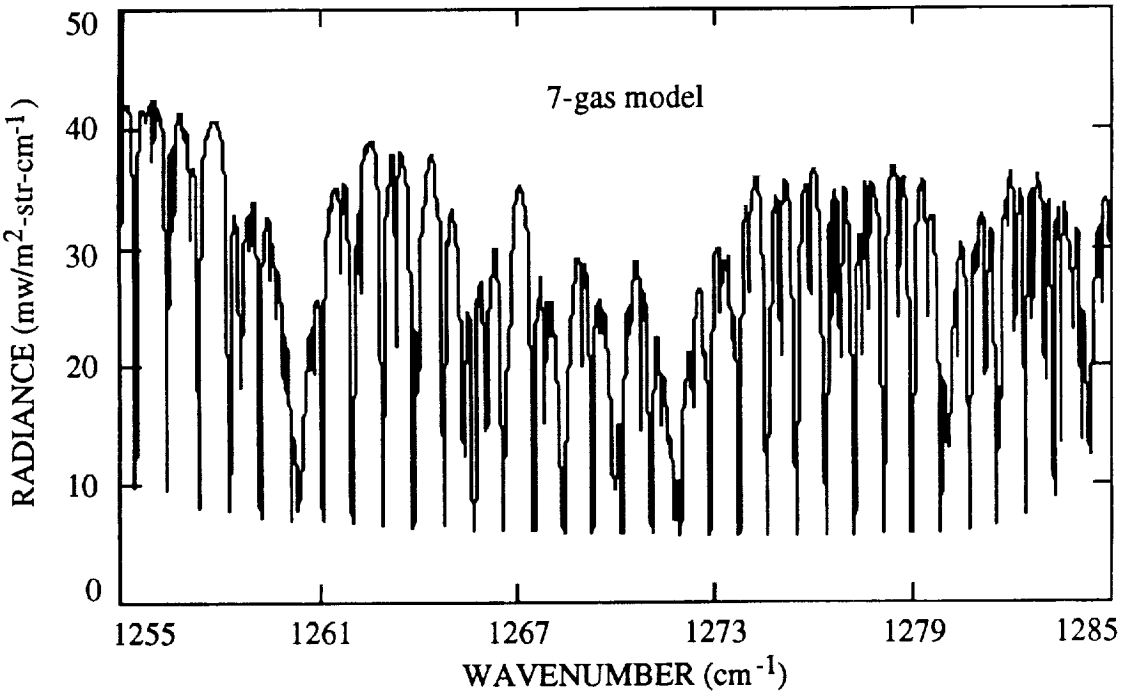

Fig. 3.11 Upwelling atmospheric radiance in N_2O band with interferences by other species. 1976 U. S. Standard Atmosphere and N_2O profile have been used in the calculation.

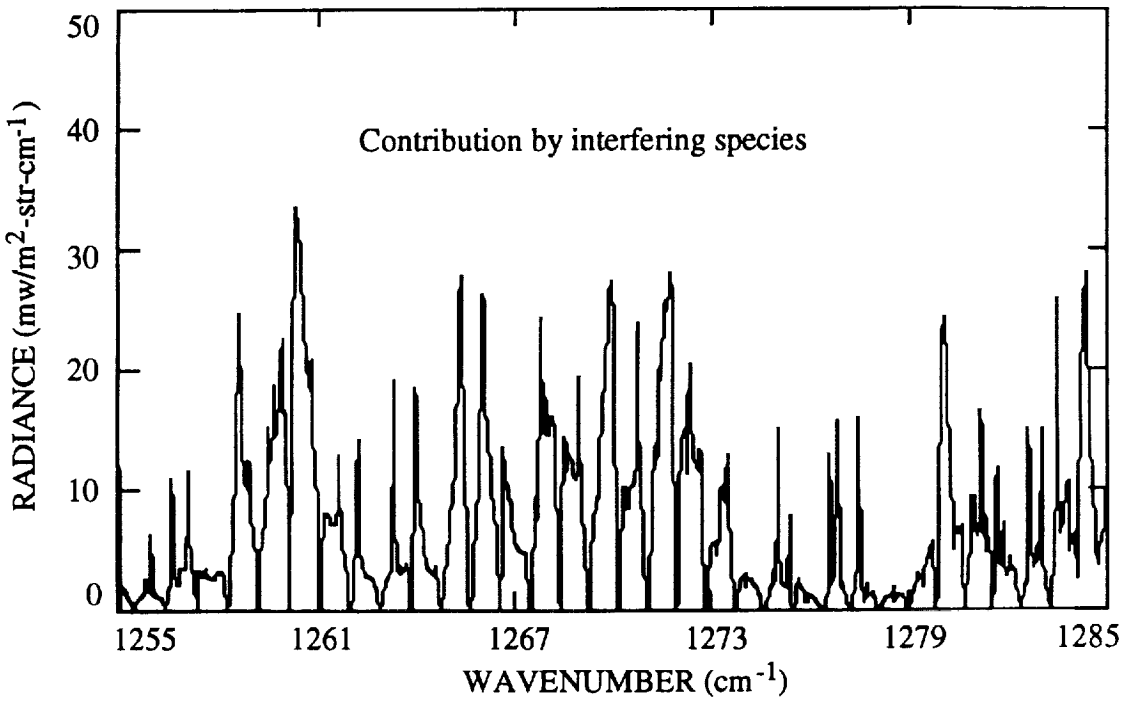

Fig. 3.12 Difference of upwelling atmospheric radiance in N_2O band with and without interferences by other species (H_2O, CO_2, O_3, CO, N_2O, O_2).

use this spectral region for N_2O sensing. The next N_2O band we examined is from 1255.0 cm^{-1} to 1285.0 cm^{-1}, the upwelling atmospheric radiance with N_2O-only model and with the 7-gas model containing N_2O, H_2O, O_3, CO, CH_4, CO_2, O_2, are plotted in Fig 3.10 and Fig. 3.11, the difference between the two is shown in Fig. 3.12. Except several spikes, the effects of other molecules (H_2O, O_3, CO_2, CH_4, CO, O_2) on the total upwelling atmospheric radiance is minimum from 1274.0 cm^{-1} to 1280.0 cm^{-1}. The contribution of solar radiation is negligible in this spectral region. The band blocking filter needed to isolate this spectral region will have a FWHM of 0.037 μm and a central wavelength of 7.833 μm, which corresponds to a relative band width of 0.47%. Consultation with the Optical Coating Laboratory (OCLI) shows that this kind of filter can be produced with the present technology. Considering all those factors, we will choose the N_2O band from 1273.0 cm^{-1} to 1279.5 cm^{-1} for MOES N_2O sounding. The upwelling atmospheric radiance in the N_2O sensing band is shown in Fig. 3.13, 7 N_2O lines are included in this band and they will be simultaneously measured and multiplexed by MOES. Figure 3.14 shows the position of the MOES N_2O sounding channels. Figure 3.15 - 3.17 show the weighting and contribution functions of the 6 N_2O sounding channels with different N_2O mixing ratio profiles. The shapes and peaking altitudes are sensitive to the changes of the N_2O mixing ratio profile. This indicates that useful information about the distribution of

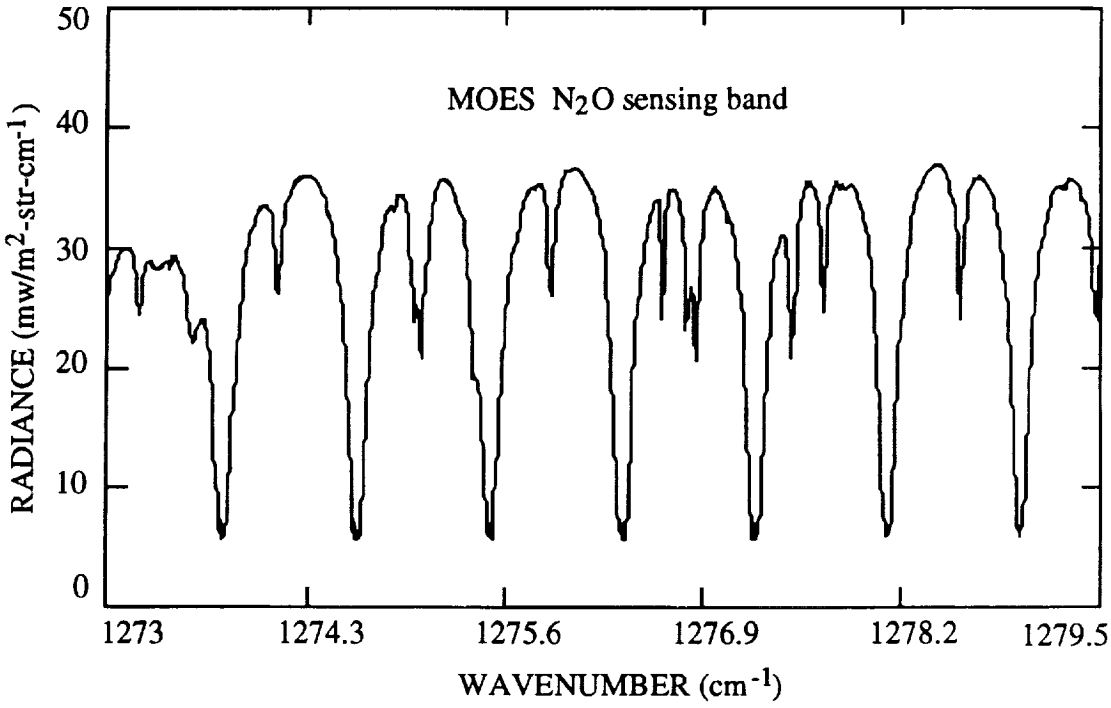

Fig. 3.13 Upwelling atmospheric radiance in MOES N_2O sensing band. 7 orders are used.

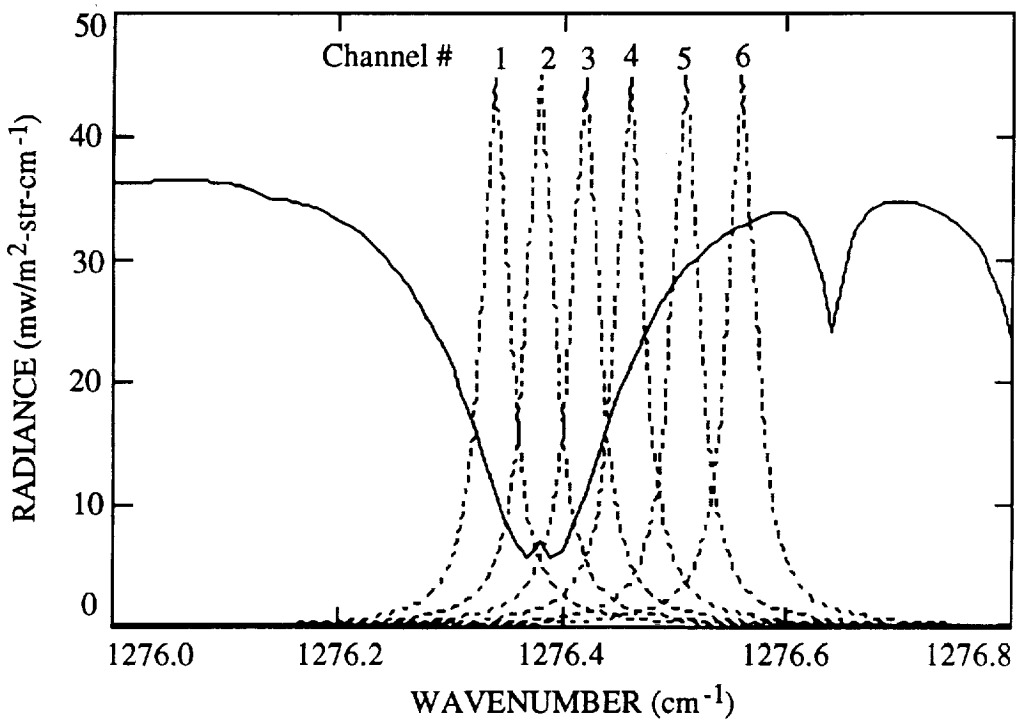

Fig. 3.14 6 MOES N_2O sensing instrument channel positions within one order.

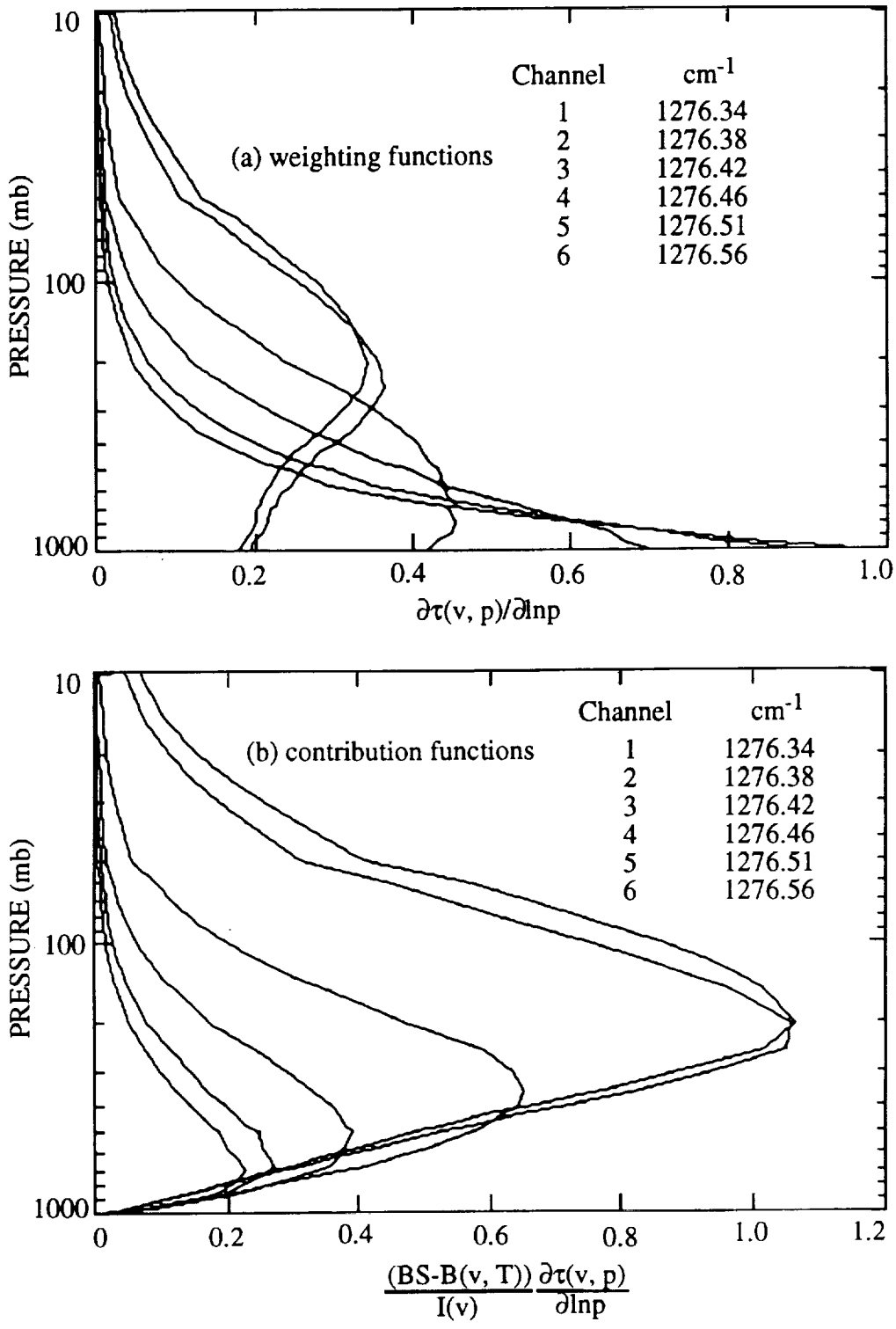

Fig. 3.15 Weighting and contribution functions of the 6 MOES N_2O sensing channels with 0.8 times the 1976 standard N_2O mixing ratio and instrument finesse of 50. BS is the surface contribution to the upwelling radiance, I(v) is the radiance "measured" by MOES.

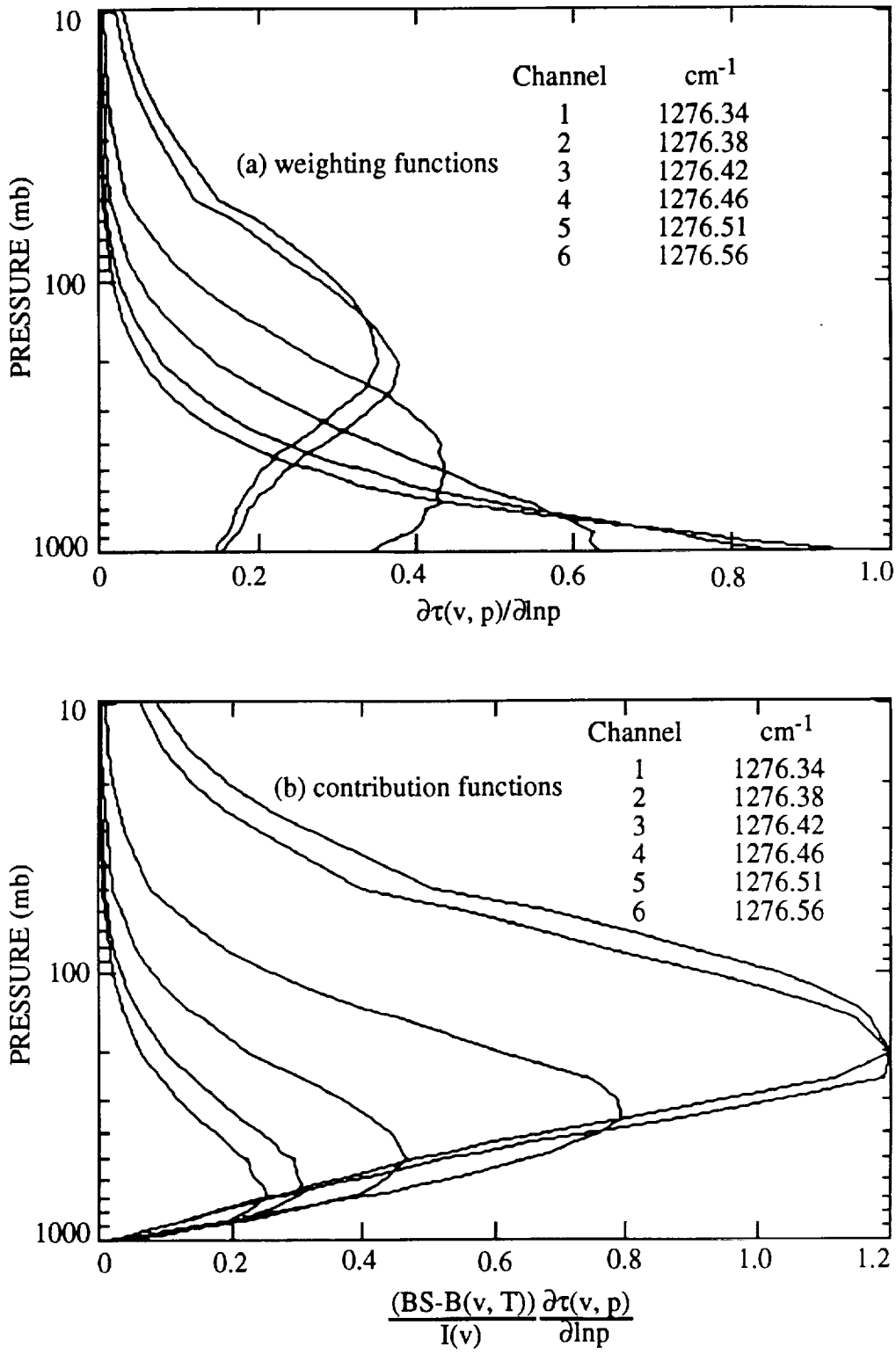

Fig. 3.16 Weighting and contribution functions of the 6 MOES N_2O sensing channels with the 1976 standard N_2O mixing ratio and instrument finesse of 50. BS is the surface contribution to the upwelling radiance, I(ν) is the radiance "measured" by MOES.

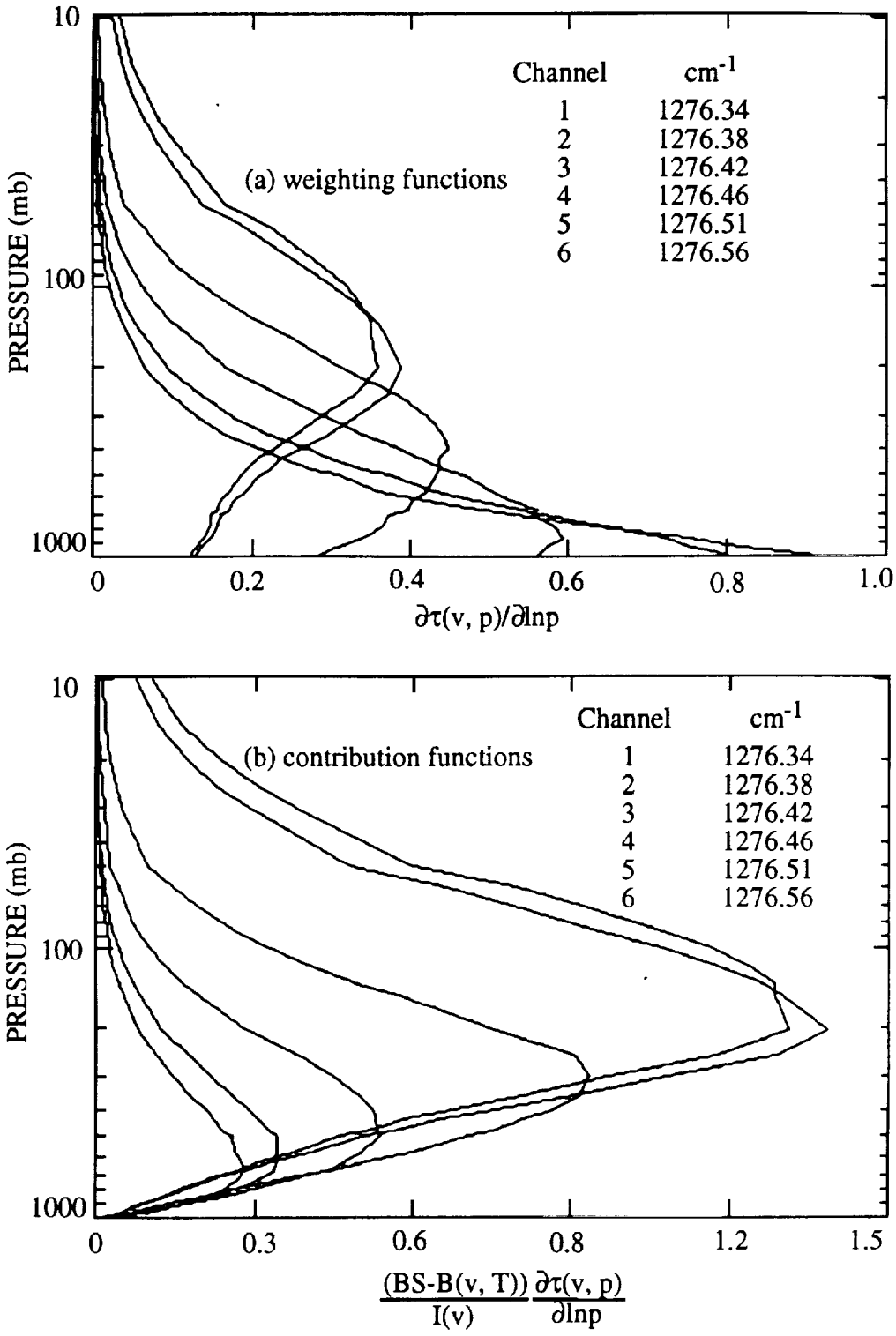

Fig. 3.17 Weighting and contribution functions of the 6 MOES N_2O sensing channels with 1.2 times the 1976 standard N_2O mixing ratio and instrument finesse of 50. BS is the surface contribution to the upwelling radiance, I(v) is the radiance "measured" by MOES.

N_2O could be derived from those measurements. The technique for the retrieval of N_2O profiles and column density from MOES measurements will be further discussed later.

3.3 Channel Selections and Requirements for Tropospheric Methane (CH_4) Measurement

CH_4 has a complicated band structure and does not have a regular spectrum as CO and N_2O. We have calculated the upwelling atmospheric radiance in several CH_4 bands, trying to find a spectral region with minimum interferences by other atmospheric species. Figure 3.18 shows the upwelling atmospheric radiance with CH_4-only model (the interferences of other species have been neglected) from 2920.0 cm^{-1} to 2950.0 cm^{-1}, which is the major CH_4 sensing region selected by AIRS on EOS. Figure 3.19 shows the upwelling atmospheric radiance with the 7 important atmospheric molecules (H_2O, O_3, CO_2, CO, N_2O, CH_4, O_2) included in the same spectral region. Fig. 3.20 shows the difference between the two, we can see there are big differences indicating that interferences by other atmospheric species in this CH_4 spectral region is quite serious. The problem with this spectral region is that solar radiation contribution to the instrument signal could be significant. Another CH_4 band we have examined is the region from 1315.0 cm^{-1} to 1345.0 cm^{-1}. Figure 3.21 shows the upwelling atmospheric radiance in this spectral region with CH_4-only model , and Fig. 3.22 shows the upwelling atmospheric radiance in the same spectral region with the 7-gas model. The difference between the spectrums with and without interferences by other atmospheric species is plotted in Fig. 3.23. We have also examined other potential CH_4 sensing spectral regions. The spectral region from 1320.0 cm^{-1} to 1335.0 cm^{-1} is chosen based on the consideration of signal, interferences by other species and solar radiation. Due to the non-regularity of CH_4 spectral spectrum, we will use the single-order approach as adopted for MOES water vapor sounding (Wang, 1990). The MOES CH_4 sensing channels are illustrated in Fig. 3.24. Weighting and contribution functions of the 10 CH_4 sensing channels are illustrated in Fig. 3.25.

3.4 MOES Tropospheric Temperature Sounding Channels

Tropospheric temperature profile is needed to retrieve the CO, N_2O and CH_4 distribution profiles. Depending on whether or not the temperature profiles are available from other instruments on the same GOES platform or from other sources, tropospheric temperature and water vapor sensing channels might need to be included in MOES. The MOES temperature and moisture sounding feasibility and capabilities have been studied before (Wang, *et al.*, 1990,1991), so only some of the results are included. Since the main objective of this project is the investigation of the feasibility of MOES for tropospheric trace

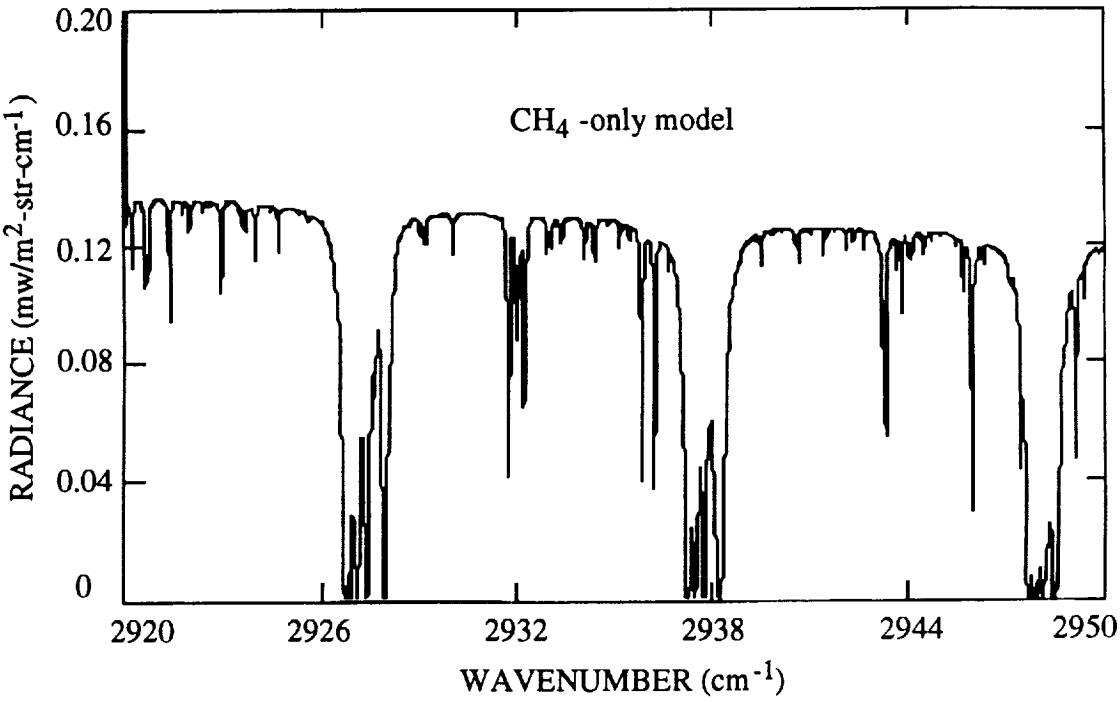

Fig. 3.18 Upwelling atmospheric radiance in the CH_4 band with CH_4-only model (no interference by other species).

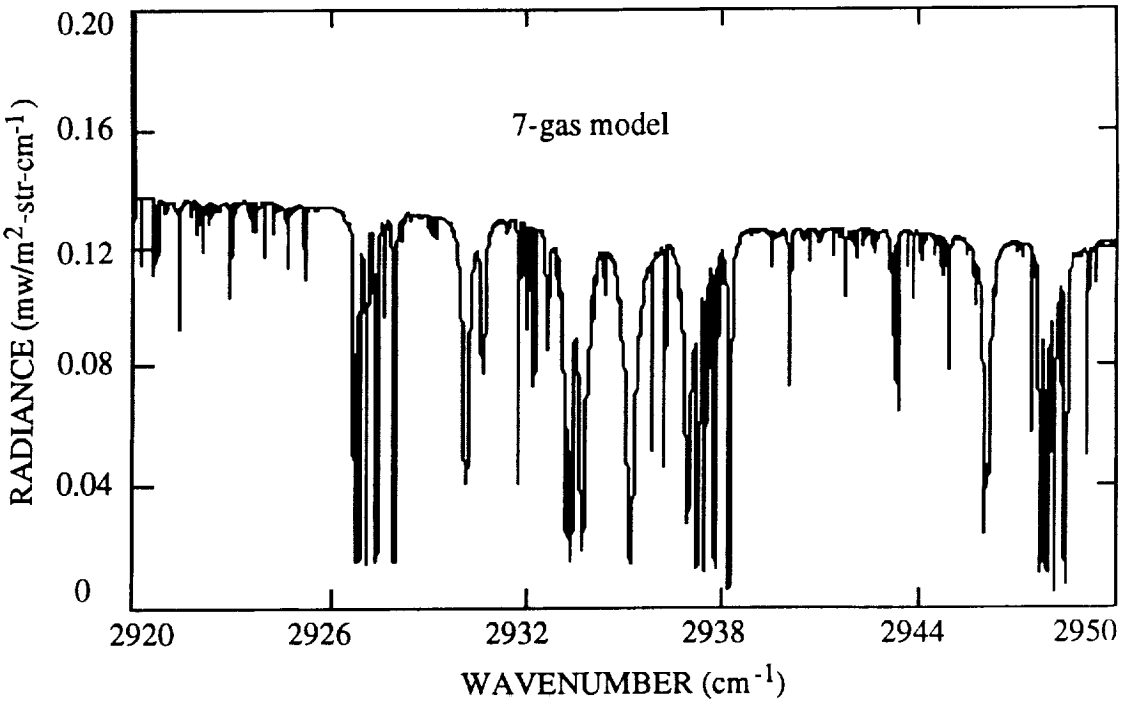

Fig. 3.19 Upwelling atmospheric radiance in the CH_4 band with 7-gas model (H_2O, CO_2, O_3, CO, N_2O, CH_4, O_2).

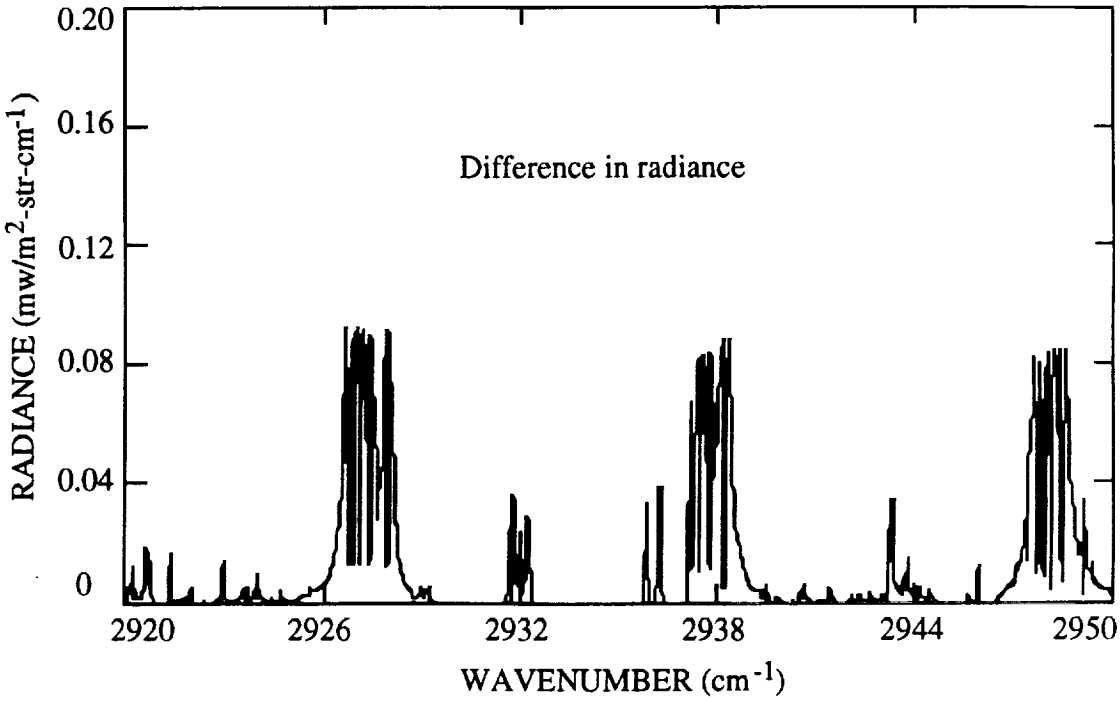

Fig. 3.20 Difference in the upwelling atmospheric radiance in the CH_4 band between the CH_4-only model and the 7-gas model (H_2O, CO_2, O_3, CO, N_2O, CH_4, O_2).

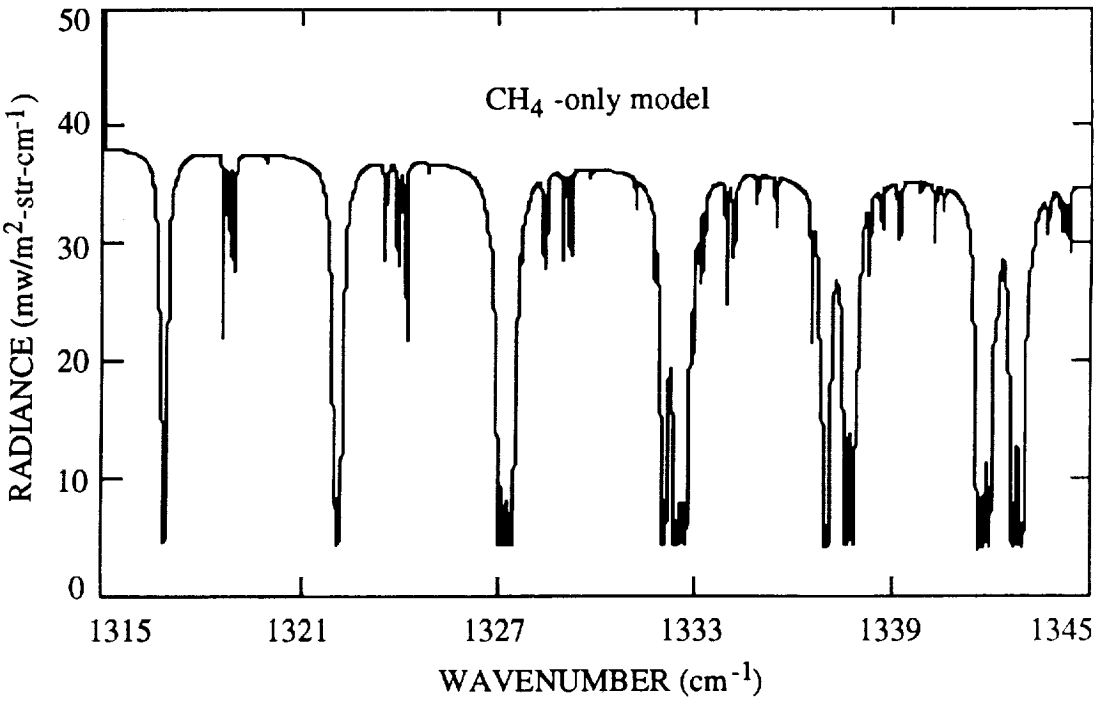

Fig. 3.21 Upwelling atmospheric radiance in the CH_4 band with CH_4-only model (no interference by other species).

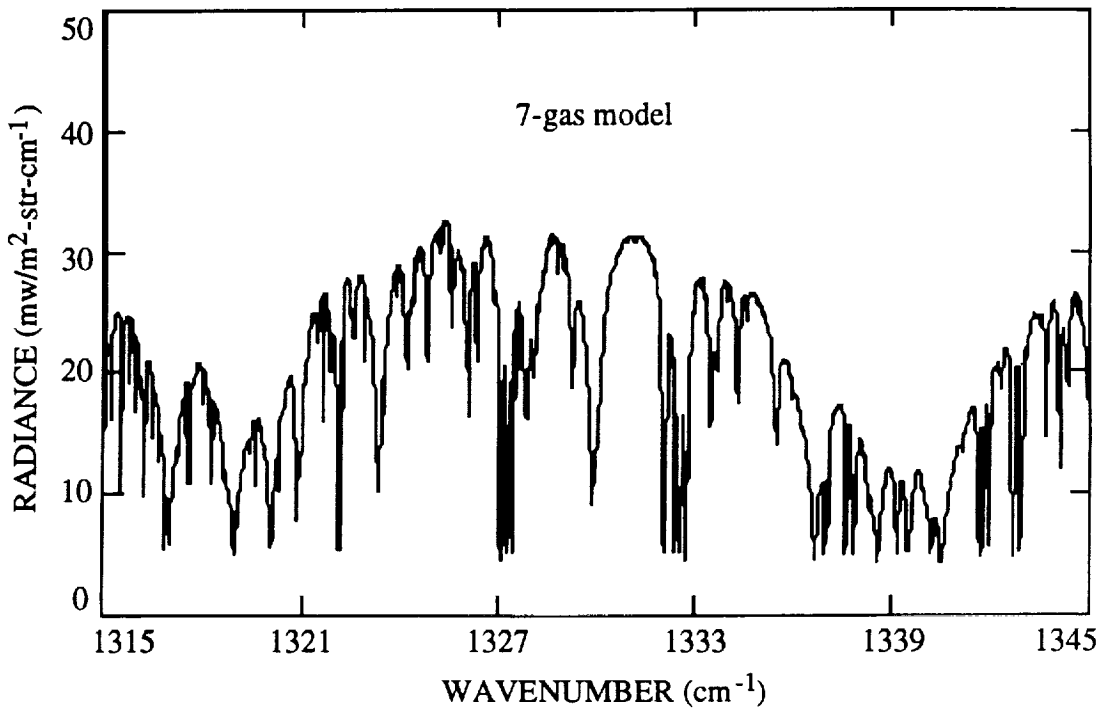

Fig. 3.22 Upwelling atmospheric radiance in the CH_4 band with 7-gas model (H_2O, CO_2, O_3, CO, N_2O, CH_4, O_2).

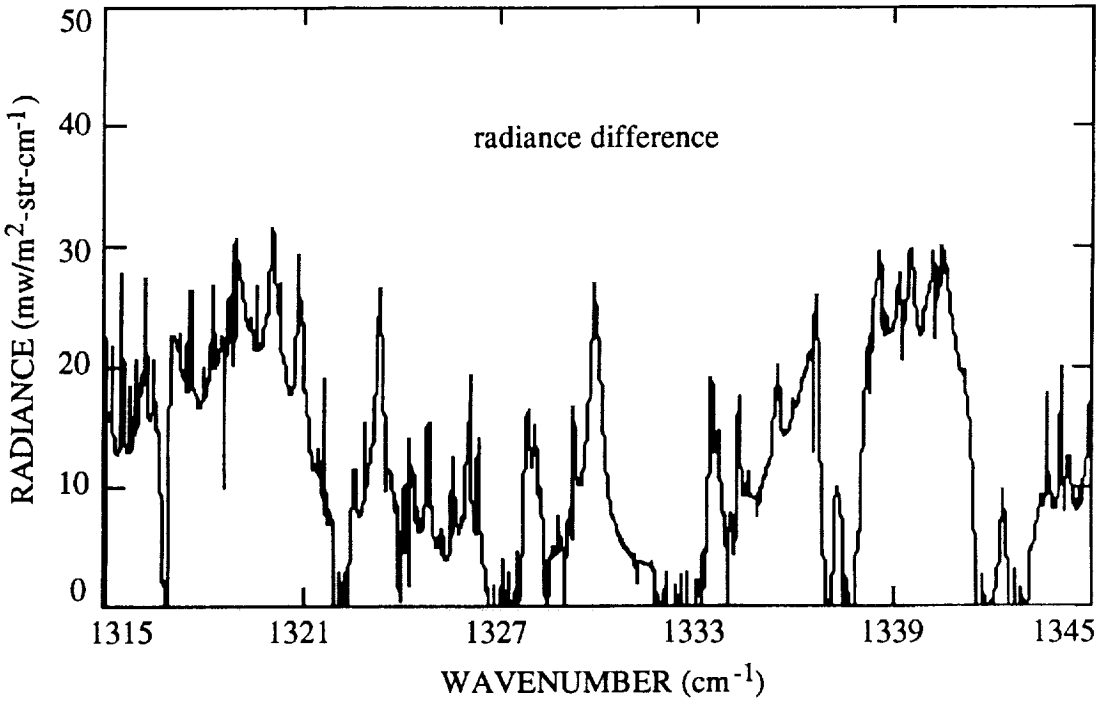

Fig. 3.23 Difference in the upwelling atmospheric radiance in the CH_4 band between the CH_4-only model and the 7-gas model (H_2O, CO_2, O_3, CO, N_2O, CH_4, O_2).

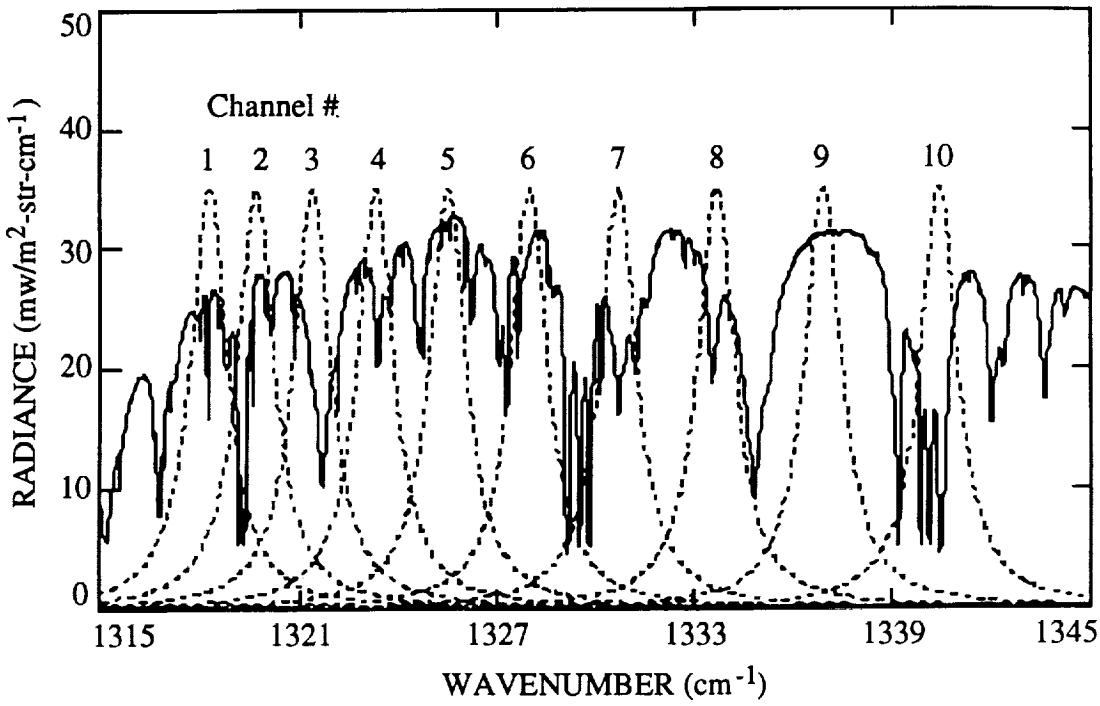

Fig. 3.24 Illustration of MOES CH_4 sensing channel positions and instrument functions with a finesse of 30.

species sensing, no detailed discussion of temperature and moisture sounding will be presented. In the retrieval simulation which will be presented in section 5, it will be assumed that temperature profiles are available. MOES can provide the tropospheric temperature profile by including a CO_2 band. The CO_2 spectral region from 725.0 cm^{-1} to 747.0 cm^{-1} is chosen for the tropospheric temperature sounding. Figure 3.26 shows the high spectral resolution upwelling CO_2 thermal emission spectrum and the weighting functions of 16 MOES temperature channels.

3.5 MOES Tropospheric Moisture Sounding Channels

Moisture profile is needed to correct its interference on the temperature sounding channels. Passive remote sensing of water vapor from satellites in the infrared can be accomplished from the 6.3 μm vibrational-rotational band of H_2O. A portion of the H_2O spectrum and the weighting functions of the 10 possible MOES moisture channels are shown in figure 3.27.

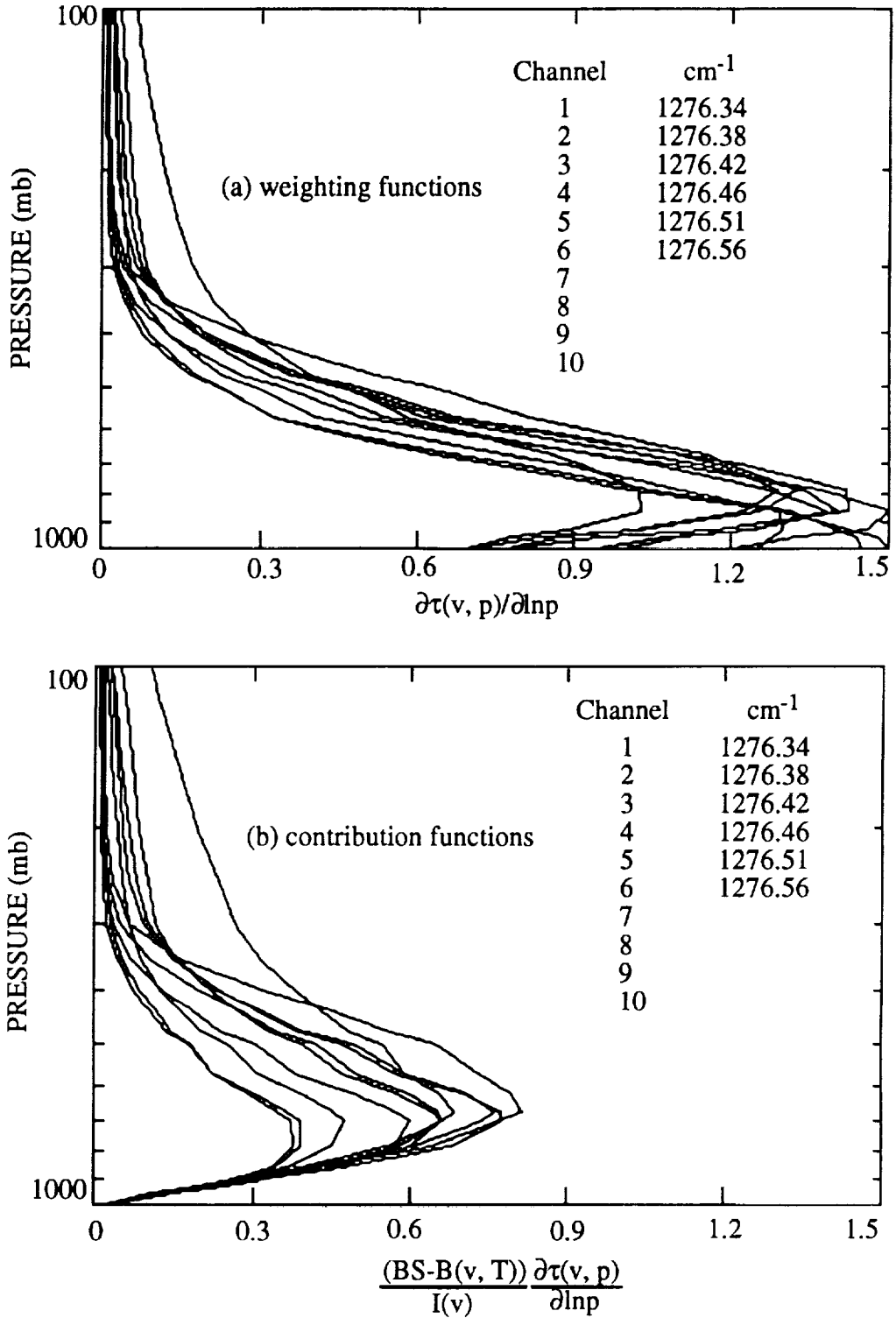

Fig. 3.25 Weighting and contribution functions of the 10 MOES CH_4 sensing channels with the 1976 standard CH_4 mixing ratio and instrument finesse of 50. BS is the surface contribution to the upwelling radiance, I(v) is the radiance "measured" by MOES.

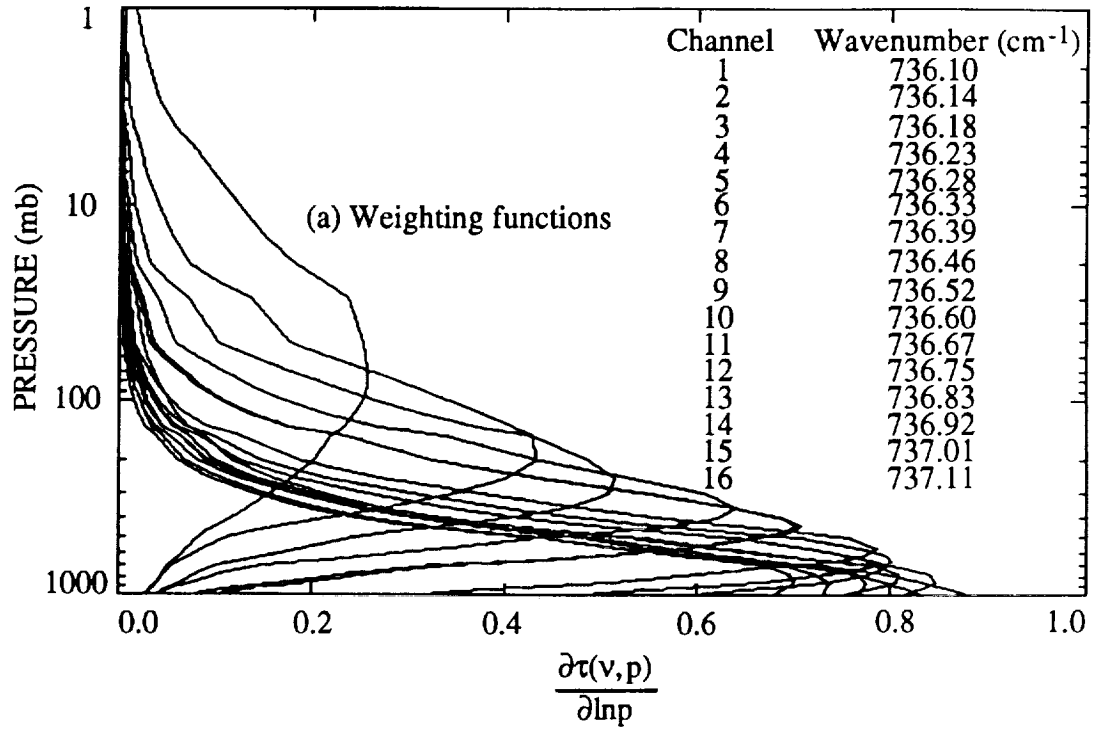

Fig. 3.26. Weighting functions of the MOES tropospheric temperature sounding channels. They are optional depending on the availability of temperature information from other sources.

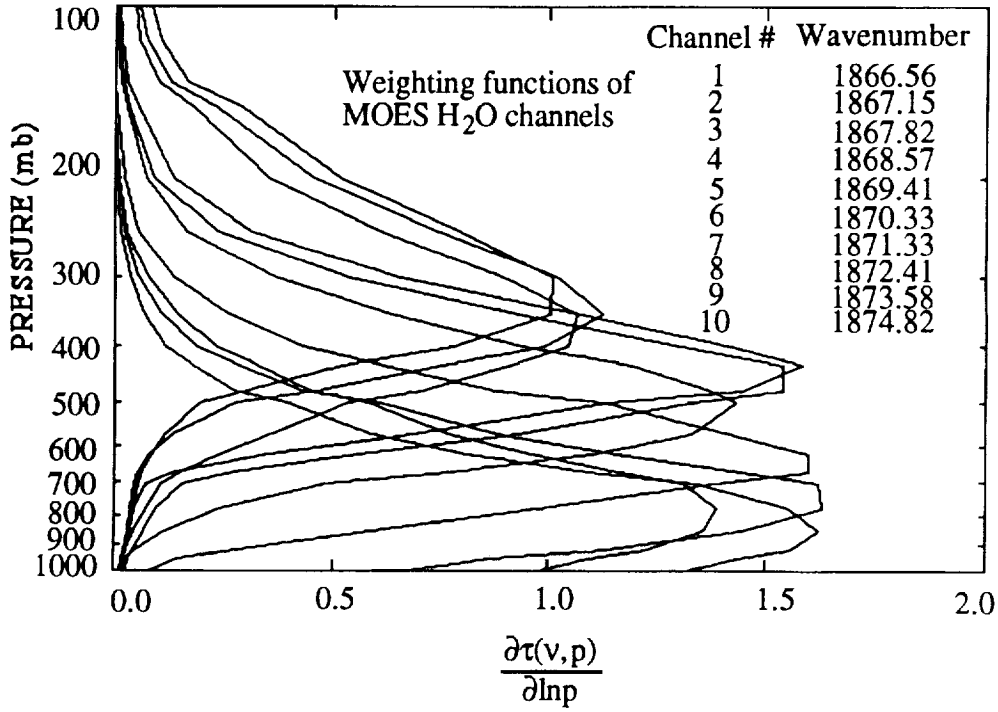

Fig. 3.27. Weighting functions of the MOES moisture sounding channels. They are optional depending on the availability of temperature and moisture information from other sources.

4.0 MOES Instrument Design Considerations

4.1 System Concept and Baseline Instrument Design

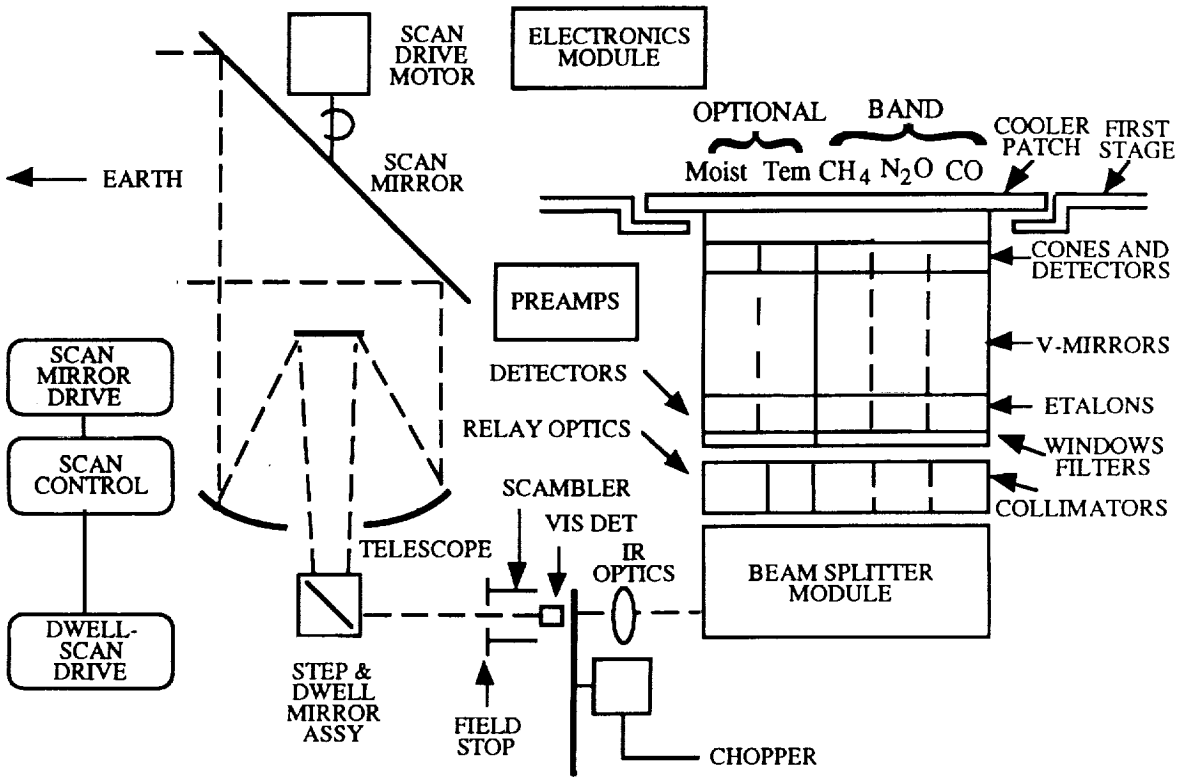

Fig. 4.1 Schematic diagram of the baseline design major MOES configuration elements. The combination of etalon assemblies and optics would provide the outputs for the CO, N_2O, CH4, temperatureand moisture sounding channels simultaneously.

The optical system design efforts will be focused on maximizing system performance and providing a flexible, compact design which is producible with today's technology. Several optical system layouts/concepts and variations have been examined. The optical system layout schematic shown in Fig. 4.1 is compatible with existing detector and etalon technology. The combination of etalon assemblies and optics will provide outputs for the CO sounding band (CO: 2152.0 cm^{-1} - 2161.0 cm^{-1}), N_2O sounding band (1273.0 cm^{-1} - 1280.0 cm^{-1}), CH_4 sounding band (1320.0 cm^{-1} - 1335.0 cm^{-1}), the optional tropospheric temperature sounding band (CO_2: 725.0 cm^{-1} - 747.0 cm^{-1}), and the optional moisture band (H_2O: 1865.0 cm^{-1} - 1879.0 cm^{-1}) discussed in previous sections. The heart of the instrument is the Fabry-Perot etalon that performs the high resolution spectral analysis of thermal radiation from the earth's atmosphere. All MOES channels will

Table 4.1: MOES Spectral Channels and Optical System Parameters

Instrument field of view (IFOV):	1.604 degree (28 mr)				
Entrance aperture diameter:	16 inch (40.64 cm)				
Instrument throughput:	0.799 $cm^2 sr$				
Band Purpose	CO Band	N_2O Band	CH_4 Band	Trop. Temp	Moisture
Spectral Band (cm^{-1})	2152 -2161	1273 -1280	1320 -1335	725 - 747	1865 - 1879
Spectral band (μm)	4.647-4.628	7.855-7.813	7.576-7.491	13.79-13.39	5.36-5.32
Band Center (μm)	4.637	7.834	7.533	13.59	5.34
Number of Chanels	10	6	10	16	10
Etalon free spectral Range (cm^{-1})	3.708	0.871	20.0	1.53	17.93
Etalon Finesse	50	30	30	30	25
Etalon Diameter (cm)	1.0	1.0	1.0	3.2	3.2
Number of orders	2	7	1	15	1
Effective System F/#	3	3	3	1.5	1.5
Lens Focal Length (cm)	7.0	7.0	7.0	11.7	11.7
Optical Transmissivity	0.25	0.25	0.25	0.25	0.25
Chopping Factor	2.5	2.5	2.5	2.5	2.5
Linear Array Detector	HgCdTe	HgCdTe	HgCdTe	HgCdTe	InSb
Element size (μmxμm)	100x500	100x1000	350x1000	250x2000	500x2000
Detector pitch (μm)	125	120	700	275	1000
Spec. Resolution (cm^{-1})	0.09 - 0.12	0.05 -0.06	0.74 - 1.03	0.07-0.11	0.7 - 1.0
D* Requirement (10^{11})	3.3 - 1.8	3.6 - 2.0	0.58 - 0.42	0.08-0.05	0.2 - 0.06
NEΔT (k) at 260 k	0.2	0.2	0.2	0.2	0.2
Integration Time (s)	1.0	1.0	1.0	1.0	1.0

share a common scan mirror and telescope primary and view the earth's atmosphere and space alternatively via a rotating double-sided mirror chopper. Individual channels are defined by the band limiting filter-etalon-lens-mirror-cone assemblies and the corresponding linear array detectors. All the five (or three without temperature and moisture channels) filter-etalon-lens-mirror-cone assemblies with their associated linear array detectors will be placed in a single dewar cooled to 80 K by a passive radiative cooler. This approach greatly reduces the optical background noise and increases the MOES system sensitivity.

The key technologies which will be incorporated into the MOES design include : (1) high resolution through the use of Fabry-Perot etalon; (2) high sensitivity through the multiplexing of orders, circle to line conversion of the etalon fringe pattern, and simultaneous sampling of all spectral bands and channels; (3) step and dwell mirror to eliminate image blur; (4) passive radiative cooling for reliability and to eliminate the vibration noise associated with sterling-cycle cryogenic coolers. Important system design parameters are listed in Table 4.1. The tropospheric temperature and moisture bands are optional depending on the availability of temperature profiles needed for the retrieval of CO, N_2O, and CH_4 profiles.

4.2 Etalon Design

The Fabry-Perot etalon is the key component of MOES. There are several options in the etalon design, the fixed air gap etalon, the solid etalon, or a piezoelectric controlled etalon. The advantages, disadvantages, and the state-of-the-art technologies in producing those etalons are described below.

Fixed Air Gap Etalon

Fixed air gap etalon is a reasonably matured technology, the Space Physics Research Laboratory has a lot of experience in working with fixed air gap etalon because the etalons in both the Dynamics Explorer (DE) Fabry-Perot interferometer and the High Resolution Doppler Imager (HRDI) on the Upper Atmospheric Research Satellite (UARS) are fixed air gap etalons. The etalons for DE-FPI and HRDI are for the visible, the etalon plates are of fused silica, and the spacer posts and the plates can be optically contacted. The etalons in MOES are for the infrared, the appropriate etalon plates material is ZnSe. The properties of ZnSe make it impossible to optically contact the plates and the spacer posts. In order to produce a fixed air gap etalon with ZnSe, other methods of contacting the posts and the plates are needed. We could use super glue to put them together, but once they are glued together, it is impossible to take them apart without destroying the plates. Since it might take several iterations to get the correct etalon, this approach may greatly raise the cost of the etalons. The most promising technique is the thermally stable, kinematic mount developed for the Dynamics Explorer mission (Killeen, Hays, et al., 1982). Another possible approach is to make a special etalon holder to hold the etalon together and keep the two plates parallel via feedback control. This approach has been used before, such as the tunable etalon produced by Queensgate Instrument Ltd..

Solid Etalon

Solid etalon is potentially a very easy and cost effective technology, but the free spectral range requirements of some of the etalons result in very thin solid etalons. For example, the optimum free spectral range for the CO band etalon is 3.708 cm^{-1}. With ZnSe refractive index of 2.40, the thickness of the solid etalon is d = 1/(2x3.708x2.40) = 0.056 cm = 0.56 mm. This is not impossible, Perkin Elmer has produced even thinner etalons. One has to be very careful in dealing with those very thin etalons and special holders are needed. Another disadvantage of the solid etalons is that the etalon gap can not be adjusted. Since in our application, certain adjustments of the etalon gaps are needed to get the correct gap thickness and channel positions, especially in the laboratory calibration stage, we recommend not to use the solid etalons approach.

Piezo-electrically Tuned Fabry-Perot Etalon

Queensgate Instruments Ltd. can provide Fabry-Perot etalons that can be cooled to cryogenic temperature for infrared Fabry-Perot interferometry (Atherton, 1988). The etalons are piezo-electrically tuned and servo-stabilized to achieve high levels of stability. Piezo-electric actuators are cemented between the mirrors giving an etalon which is tunable by up to 15 orders of interference about a nominal fixed cavity length. Etalons with clear apertures from 28mm to 140mm are available fabricated in ZnSe for 3 to 15 μm spectral region. The etalons are cell mounted with flying leads for ease of mechanical and electrical installation. This new piezo-electrically tuned etalon for low temperature operation is a very good option for our purpose and provide an alternative for the fixed air gap etalon.

4.3 Detectors

Detector Selections and Configurations

Five linear array detectors will be needed to cover the CO sounding band, the N_2O sounding band, the CH_4 sounding band, the tropospheric temperature sounding band, and the water vapor sounding band. Consultations with several IR detector manufactures (EG&G Judson, Infrared Associates, Electro-Optical Systems) indicate that detectors are readily available to meet our requirements. The sizes and pitches of the detector elements directly affect the effective channel spectral resolutions and the number of channels in each bands. Large detector sizes and pitches provide better signal-to-noise, but reduce the effective channel spectral resolutions and the number of channels that can be used. Depending on sensitivity requirements, either uniform linear array (all the elements within the linear array are of the same size and pitch) detectors or nonuniform linear array detectors (detector elements within the linear array are of different sizes and pitches) could

be used. Therefore, careful studies are needed to define the configuration, detector element sizes, and detector pitches of each of the line array detectors.

Detector Cooling Considerations

Infrared detectors must operate at low temperature to reduce inherent noise. The use of very narrow band spectral blocking filters at detector temperature in MOES will make the detectors to be either detector noise limited or pre-amplifier noise limited. Both the cryogenic refrigerator system and the passive radiative cooler can keep the detectors at about 80 K. In our preliminary design, we choose the passive radiative cooler approach because of its reliability and the possible long duration of the satellite remote sensing mission. Although mechanical coolers could also be used, but we prefer the radiative cooling approach. The TIROS experience has shown that modern IR sounders are sensitive to vibration noise generated by on-board mechanical coolers. So care must be taken in the utilization of mechanical coolers.

4.4 Circle-to-Line Optics (CLIO) Design Considerations

Preliminary design of the CLIO, or the kaleidoscope and cone assembly, has been carried out at SPRL. First, a laboratory design tolerance study was undertaken. The purpose of the laboratory design tolerance study is to demonstrate the overlapping of the four segments of the interference fringes, the conversion of one quarter of the circular fringe into a narrow line segment as predicated by theory and ray trace, and the mechanical and optical tolerance on the kaleidoscope and cone design. The results of the design study and consultation with several metal optics suppliers (such as the Speedring Systems) indicate that the CLIO can be manufactured cost effectively by single-point diamond machining technology. A picture of the kaleidoscope-cone assembly produced by single-point diamond turning for tropospheric temperature sounding band is shown in Fig. 4.2.

Fig. 4.2. Pictures of the kaleidoscope-cone assembly produced by single-point diamond turning. The picture at the bottom shows the Kaleidoscope-cone-lens-etalon assembly.

5.0 Retrieval Algorithm Development

During the selection of retrieval method and development of retrieval algorithm process, different techniques have been tried and compared. First, the iteration technique by Chahine (Chahine, 1972) was tried, and the results are not very satisfactory. The reason that we did not get good results with this technique is that most of the weighting functions peak close to the ground, and the peaks of some of the weighting functions are not very well defined, but in the iteration technique by Chahine the mixing ratios of the specy at the peak positions of the weighting functions are iterated. We have also tried the linear inversion technique of Smith (Smith et al., 1991) without much success. The main reason for this is that some assumptions in the linearization process are not valid in our case. Later on, we decided to use the optimal estimation method described by Rodgers (Rodgers, 1976, 1990). The technique and its application to MOES are briefly described here. The detailed explanation of the method can be found in the paper.

The radiative transfer equation is given below

$$I(\nu, z_{obs}) = I(\nu, z_s)\tau(\nu, z_s, z_{obs}) + \int_{z_s}^{zobs} [B(\nu, T(z))k(\nu, z)\rho_a(z)dz]\tau(\nu, z, z_{obs}) \qquad (5.1)$$

where $I(\nu,z)$ is the radiation intensity in $W/(m^2.sr.cm^{-1})$, $\rho_a(z)$ is the absorber (such as CO, N_2O, CH_4, ...) number density in $molecules.cm^{-3}$, and $k(\nu,z)$ is the monochromatic absorption coefficient in $1/(molecules.cm^{-2})$. After convolving the above equation with the MOES instrument function and re-arrange the equation , we get

$$Y = F(X) \qquad (5.2)$$

where Y is the vector related to the measured radiance by the instrument, it is the known vector, X is the unknown vector containing the mixing ratios of CO, N_2O, or CH_4. By expanding the forward model (equation (5.2)) as a Taylor series about a guessed value of X_n of the solution, we get

$$Y = F(X_n) + \partial F / \partial X \, (X - X_n) + 0(X - X_n) \qquad (5.3)$$

By re-defining $F(X_n)$ as Y_n, and $\partial F/\partial X$ as K_n, we get

$$Y = Y_n + K_n(X - X_n) + 0(X - X_n) \qquad (5.4)$$

The higher-order terms are ignored, so that a set of under-constrained linear equations for X remains, which can be solved by the Newtonian Iteration technique. The solution is updated from X_n to X_{n+1} by the following equation

$$X_{n+1} = X_0 + S_X K_n^T (K_n S_X K_n^T + S_\varepsilon)^{-1} [Y - Y_n - K_n (X_0 - X_n)] \quad (5.5)$$

where X_0 is the first guess vector (apriori information) of the species (CO, N_2O, or CH_4) profile, Y is the "measured" or "true" signal (e.g. radiance) (Y=F(X)), Y_n is the calculated signal in the iteration process (Y_n=F(X_n)), $K_n = \partial F/\partial X$ = Frechet derivative, it can be calculated analytically or computed numerically by perturbing the forward model, S_X is the covariance matrix of the apriori information, and S_ε is the covariance matrix of the measurement. The iteration process is stopped if the convergence criterion is met, such as Y_{n+1}-Y_n or X_{n+1}-X_n is small enough. In summary, the procedures of deriving atmospheric trace species from MOES measurements based on the iteration scheme in equation (5.5) are:

(1) Develop forward model Y = F(X) based on the radiative transfer equation so that signal or radiance can be calculated from the species profiles. In this process, line by line transmittance and radiance models, we have used the SPRL line-by-line code initially developed by Drayson and the FASCOD2 developed by AFGL in our study.

(2) Calculate Frechet derivative "K" through perturbation of the forward model one atmospheric level at a time to get "K" matrix. This process could be time consuming and CPU intensive depending on the number of levels of the atmosphere used in the forward calculation.

(3) Formulate covariance matrices of species S_X of interest based on aprior information.

(4) Formulate covariance matrix of the measurement S_ε.

(5) Use equation (5.5) to get next guess X_{n+1}. Repeat until the "calculated" signal Y_{n+1} converges to the "measured" signal, i.e. convergence criterion is satisfied.

We note here that our retrieval simulation by using the optimal estimation method is still in progress. More work are needed to assess the capability of MOES for the remote sensing of tropospheric trace species.

6.0 Summary and Recommendations

The remote sensing of tropospheric trace species are very important in our understanding of the global atmosphere and the implications of human activities to the atmospheric environment. Despite many years of efforts, data on the global distribution of the key tropospheric trace species, such as CO, N_2O, CH_4, are almost non-existent. Several techniques to remotely measure the distribution of tropospheric trace species have been discussed in the scientific community and federal agencies. We believe the technique of using the high resolution, high throughput Fabry-Perot interferometer is a very promising one. Our feasibility study shows that MOES , as a combination of the high resolution Fabry-Perot interferometer and the new circle to line converter, is a feasible new approach to high spectral resolution tropospheric trace species sensing. Suitable spectral regions and instrument channels for the remote sensing of tropospheric CO, N_2O, CH_4 have been discussed. Weighting and contribution functions have been calculated. Conceptual instrument design shows that MOES is within the capability of present technique. The FPI has a proven record on spacecraft. MOES has a small data rate and low power requirement.

We recommend that a feasibility demonstration on the balloon platform to be carried out as soon as possible. The balloon MOES instrument will enable us to further evaluate the new technique and could also provide measurements for the evaluation of EOS instrument performance.

References

Atherton, P., "Fabry-Perot Interferometer," *Instrumentation for Ground-Based Optical Astronomy,* 125-133, Springer-Verlag New York Inc., 1988.

Chahine, M. T., "A General Relaxation Method for Inverse Solution of the Full Radiative Transfer Equation," *J. Atmos. Sci.*, **29**, 960, 1970.

Dickinson, R. E., and R. J. Cicerone, "Future Global Warming from Atmospheric Trace Gases," *Nature,* **319**, 109,1986.

Drummond, J. R. and A. Ashton, Radiative Measurements of Pressure Modulator Operation, *J. Atmos. Oceanic Technol.*, 187-194, 1990.

Hays, P. B., T. L. Killeen, and B. C. Kennedy, "The Fabry-Perot Interferometer on Dynamics Explorer," *Space Sci. Inst.*, **5**, 395-416, 1981.

Hays, P. B., "High Resolution Doppler Imager (HRDI)," *Upper Atmosphere Research Satellite (UARS) Mission.* Goddard Space Flight Center, Greenbelt, Maryland, May, 1985.

Hays, P. B., "Circle to Line Interferometer Optical System," *Appl. Opt.*, **29**, 1482-1489, 1990.

Hernandez, G., *Fabry-Perot Interferometers*, University Press, Cambridge, 1986.

Herzberg, G., *Molecular Spectra and Molecular Structure 1: Spectral of Diatomic Molecules*, Van Nostrand, New York, 1950.

Isaksen, I. S., and F. Stordal, "Ozone Perturbations by Enhanced Levels of CFCs, N_2O, and CH_4: A Two-Dimensional Diabatic Circulation Study Including Uncertainty Estimates," J. Geophys. Res., **91**, 5249, 1986.

Jacquinot, P., The Luminosity of Spectrometers with Prisms, Gratings or Fabry-Perot Etalons, *J. Opt. Soc. Am.*, **44**, 761-765, 1954.

Khalil, M. A. K., R. A. Rasmussen, "Carbon Monoxide in the Earth's Atmosphere: Increasing Trend," *Science,* **224**, 54-56, 1984.

Killeen, T. L., B. C. Kennedy, P. B. Hays, D. A. Symanov, and D. Ceckowski, Image Plane Detector for the Dynamics Explorer Fabry-Perot Interferometer, *Appl. Opt.*, **22**, 3503-3513, 1983.

Levin, J. S., "Space Opportunities for Tropospheric Chemistry Research," *NASA Conference Publication 2450*, 1987.

Logan, J. A., M. J. Prather, S. C. Wolfsy, and M. B. McElroy, "Tropospheric Chemistry: A Global Perspective," *J. Geophys. Res.*, **86**, 7210-7254, 1981.

May, R. D., D. J. McCleese, D. M. Rider, J. T. Schofield and W. R. Webster, Tunable Diode Laser Spectral Diagnostic Studies of a Pressure Modulator Radiometer, *Appl. Opt.*, **27**, 3591-3593, 1988.

Reichle, H. G. Jr., Vickie S. Connors, J. Alvin Holland, Warren D. Hypes, and H. Andrew Wallio, Middle and Upper Tropospheric Carbon Monoxide Mixing Ratios as Measured by a Satellite-borne Remote Sensor During November 1981, *J. Geophys. Res.*, **91**, 10865-10887, 1986.

Reichle, H. G. Jr., V. S. Connors, H. A. Wallio, J. A. Holland, R. T. Sherrill, J. C. Casas, and B. B. Gormsen, "The Distribution of Middle Tropospheric Carbon Monoxide During early October 1984," *J. Geophys. Res.*, **95**, 9845-9856, 1990.

Reichle, H. G. Jr., TRACER: A Multi-Level Tropospheric Carbon Monoxide Correlation Radiometer for EOS, *Optical Remote Sensing of the Atmosphere, 1990 Technical Digest*, Vol. 4, Incline Village, Nevada, February 12-15, 1990.

Reichle, H. G. Jr., H. A. Wallio, and B. B. Gormsen, Feasibility of Determining the Vertical Profile of Carbon Monoxide from a Space Platform, *Appl. Opt.*, **28**, 2104-2110, 1989.

Roche, A. E., and J. B. Kumer, Cryogenic Limb Array Etalon Spectrometer (CLAES): Experiment Overview, *SPIE Proceedings*, Vol. **973**, 324-334, 1988.

Rodgers, C. D., "Retrieval of Atmospheric Temperature and Composition From Remote Measurements of Thermal Radiation," *J. Geophys. Res.*, **14**, 609-624, 1976.

Rodgers, C. D., "Characterization and Error Analysis of Profiles Retrieved From Remote Sounding Measurements," *J. Geophys. Res.*, **95**, 5587-5595, 1990.

Smith, W. L., Harold M. Woolf, and Henry E. Revercomb, "Linear Simultaneous Solution for Temperature and Absorbing Constituent Profiles From Radiance Spectra," *Appl. Opt.*, **30**, 1117-1123.

Taylor, F. W., *Pressure Modulator Radiometry*, in Vol. III of *spectroscopic Techniques*, edited by G. A. Vanasse, Academic, New York, 1983.

Vaughan, J. M., T*he Fabry-Perot Interferometer: History, Theory, Practice and Applications*, Adam Hilger, 1989.

Wang, J., S. Roland Drayson and Paul B. Hays, Atmospheric Temperature Sensing with a Multiorder Fabry-Perot Interferometer, *Appl. Opt.*, **28**, 5038-5046, 1989.

Wang, J., S. Roland Drayson and Paul B. Hays, Atmospheric Temperature Sounding with a Multi-Order Fabry-Perot Interferometer, *Optical Remote Sensing of the Atmosphere, 1990 Technical Digest*, Vol. **4**, Incline Village, Nevada, February 12-15, 1990.

Wang, J., "An Investigation on the Multiorder Fabry-Perot Interferometer as a Satellite-Borne High Resolution Atmospheric Temperature Sounder," Ph.D. Thesis, University of Michigan, 1990.

WMO, Report No. 16, Volume I, p78.